An Immersed C^0 Interior Penalty Method for Biharmonic Interface Problems

Yuan Chen[1], Xu Zhang[2]

Abstract

In this paper, we introduce an immersed C^0 interior penalty method for solving two-dimensional biharmonic interface problems on unfitted meshes. To accommodate the biharmonic interface conditions, high-order immersed finite element (IFE) spaces are constructed in the least-squares sense. We establish key properties of these spaces including unisolvency and partition of unity are, and verify their optimal approximation capability. These spaces are further incorporated into a modified C^0 interior penalty scheme with additional penalty terms on interface segments. The well-posedness of the discrete solution is proved. Numerical experiments with various interface geometries confirm optimal convergence of the proposed method in L^2, H^1 and H^2 norms.

AMS suject classification: 35R05, 65N15, 65N30
Keywords: immersed finite element, C^0 interior penalty method, biharmonic interface problems

1 Introduction

The biharmonic equation arises from plate bending theory in continuum mechanics. Its numerical solution poses significant challenges, particularly when using conforming finite element methods, since constructing C^1-conforming elements [6] is notoriously difficult and expensive. To address this difficulty, a wide range of alternative discretization techniques have been developed over the past several decades.

One direction involves nonconforming finite element methods [38], which relax inter-element continuity requirements. However, these elements lack a systematic hierarchy to higher-order spaces. Another approach is mixed finite element methods [27, 7], which reformulate the fourth-order PDE into a system of second-order equations. While effective in some cases, the mixed formulation introduces saddle-point structures and require stable element pairs that satisfy the Ladyshenskaya–Babušhka–Brezzi (LBB) condition [13], which is often nontrivial to construct. In addition, discontinuous Galerkin (DG) methods [39, 23], weak Galerkin (WG) methods [40] are very flexible on approximation spaces and mesh types, but they usually have the very high number of degrees of freedom, which makes these method costly to use.

A balanced alternative between H^2-conforming finite elements and fully discontinuous Galerkin methods is the H^1 semi-conforming approximation, known as the C^0 interior penalty method [26, 11]. This method is particularly attractive because it uses only standard C^0 Lagrange elements while preserving the positive-definiteness of the resulting linear system and maintaining a natural hierarchy to higher order. Its flexibility

[1]Department of Mathematics, The Ohio State University, Columbus, OH 43210, USA. Email: chen.11050@buckeyemail.osu.edu

[2]Department of Mathematics, Oklahoma State University, Stillwater, OK 74078, USA. Email: xzhang@okstate.edu. This author is partially supported by National Science Foundation grant DMS-2110833

has enabled extensions to a variety of PDEs, including optimal control problems [12], phase field crystal equations [25], and Hamilton–Jacobi–Bellman equations [9], among others.

In this paper, we focus on biharmonic interface problems, governed by fourth-order elliptic equations with discontinuous coefficients across heterogeneous media. Such problems arise in composite plate bending, multiphase materials, and phase transition models. Let $\Omega \subset \mathbb{R}^2$ be an open bounded domain separated by a closed interface Γ such that $\overline{\Omega} = \overline{\Omega^+ \cup \Omega^- \cup \Gamma}$. Consider the two-dimensional biharmonic problems:

$$\Delta(\beta(\mathbf{x})\Delta u) = f, \quad \text{in } \Omega/\Gamma, \tag{1.1a}$$
$$u = 0, \quad \text{on } \partial\Omega, \tag{1.1b}$$
$$\partial_n u = 0, \quad \text{on } \partial\Omega, \tag{1.1c}$$

where the Laplacian is $\Delta := \frac{\partial^2}{\partial x_1^2} + \frac{\partial^2}{\partial x_2^2}$. $n = (n_1, n_2)$ and $t = (t_1, t_2)$ denote the outward normal and tangential unit vectors, respectively, and β is a piecewise constant coefficient that takes distinct values $\beta^{\pm}$ on $\Omega^{\pm}$. Across the interface Γ, the solution satisfies continuity conditions on the displacement and the normal derivative (see (1.1d)-(1.1e)), as well as two Neumann-type interface conditions (see (1.1d)–(1.1g)):

$$[\![u]\!]_\Gamma = 0, \quad \text{on } \Gamma, \tag{1.1d}$$
$$[\![\partial_n u]\!]_\Gamma = 0, \quad \text{on } \Gamma, \tag{1.1e}$$
$$[\![\beta\partial_{nn} u]\!]_\Gamma = 0, \quad \text{on } \Gamma, \tag{1.1f}$$
$$[\![\partial_n (\beta\Delta u + \beta\partial_{tt} u)]\!]_\Gamma = 0, \quad \text{on } \Gamma, \tag{1.1g}$$

where the jump operator $[\![v]\!]_\Gamma := v^+|_\Gamma - v^-|_\Gamma$. Here and thereafter, we denote

$$\partial_n v = \sum_{i=1}^{2} n_i \partial_i v, \quad \partial_t v = \sum_{i=1}^{2} t_i \partial_i v, \quad \partial_{nn} v = \sum_{i=1}^{2}\sum_{j=1}^{2} n_i n_j \partial_{ij} v, \quad \partial_{tn} v = \sum_{i=1}^{2}\sum_{j=1}^{2} t_i n_j \partial_{ij} v,$$

where $\partial_i = \frac{\partial}{\partial x_i}$, and $\partial_{ij} = \frac{\partial^2}{\partial x_i \partial x_j}$. For biharmonic interface problems, while the Dirichlet interface conditions (1.1d)-(1.1e) are universal, there are two types of Neumann interface conditions in the literature. The first one, derived from Stokes formulation, takes the form

$$[\![\beta\Delta u]\!]_\Gamma = 0, \quad [\![\partial_n(\beta\Delta u)]\!]_\Gamma = 0. \tag{1.2}$$

The second type is derived form the energy functional of free thin plate bending problem, which takes the form of (1.1f)-(1.1g).

The main idea of immersed finite element methods is to solve interface problems on unfitted meshes by designing special shape functions with similar behaviors as exact solutions around the interface. On the interface elements, piecewise polynomials are enforced to (weakly) satisfy jump conditions on interface. Over the past decades, the IFE method has been developed to solve elliptic equations [35, 30], elasticity systems [36, 29], Stokes equations [32, 21], and Navier Stokes equations [22, 42], to name only a few. The IFE method has been extended to higher order for solving elliptic problems through weak enforcement [2], least square construction [3], Cauchy extension [28, 1], and Frenet transformation [4, 5]. The main obstacle of high-order IFE construction is that polynomials are impossible to satisfy interface conditions exactly on general curves. The least-squares approximation provides an efficient approach to weakly impose the interface jump conditions [3, 21, 22].

Several immersed finite element approaches have been developed for biharmonic interface problems. For instance, [34, 18] employed a mixed formulation, and used piecewise linear IFE functions to approximate the resulting saddle problem. In a recent paper [19], the mixed formulation was extended to biharmonic interface problems on surfaces. The same idea has also been used in a finite difference framework [33]. In the nonconforming framework, an immersed Morley element was constructed in [17] and a Nitsche extended finite element method was developed for solving biharmonic interface problems. Nevertheless, the development of high-order IFE spaces for fourth-order interface problems remains limited.

Other methods for biharmonic interface problems on unfitted meshes have also been proposed. For example, CutFEM [14, 15, 16] use C^1 finite element space with Nitsche's method for weak enforcement of the interface conditions. A reconstructed discontinuous Galerkin method [20] has been developed using unfitted meshes, where the approximation space is constructed by patch reconstruction and the interface conditions are enforced weakly through Nitsche-type techniques. More recently, a nonconforming virtual element method on unfitted polygonal meshes has been developed in [37].

In this paper, we introduce a modified C^0 interior penalty method with immersed $\mathcal{P}_k$ finite elements for solving the biharmonic interface problem (1.1). High-order $\mathcal{P}_k$ immersed finite element spaces are constructed through a recently developed least-squares approach [3, 21]. We analyze key properties of new IFE space, such as unisolvency and partition of unity, and verify their approximation capability. These spaces are incorporated into a modified C^0 interior penalty method, in which additional penalty terms are imposed along the interface curves for stabilization. We prove the well-posedness of the numerical scheme and present extensive numerical examples to demonstrate the optimal convergence in L^2, semi-H^1 and semi-H^2 norm.

The rest of paper is organized as follows: Section 2 introduces notations and assumptions used throughout the text. Section 3 develops the high-order immersed finite element spaces and establish their fundamental properties. Section 4 presents the modified C^0 interior penalty scheme and its theoretical analysis on well-posedness. Section 5 reports numerical experiments to assess the performance of the method. Section 6 concludes with a brief summary.

2 Notations and Assumptions

In this section, we introduce some notations and assumptions to be used in this paper. Let $\tilde{\Omega} \subset \Omega$, we denote the standard Sobolev space $W^{k,p}(\tilde{\Omega})$ with norm $\|\cdot\|_{W^{k,p}(\tilde{\Omega})}$ and semi-norm $|\cdot|_{W^{k,p}(\tilde{\Omega})}$ for $k \geq 1$ and $1 \leq p \leq \infty$. For $p = 2$, we write $H^k(\tilde{\Omega})$ with norm $\|\cdot\|_k$ and semi-norm $|\cdot|_k$. If $\tilde{\Omega} \cap \Gamma \neq \emptyset$, we set $\tilde{\Omega}^s = \tilde{\Omega} \cap \Omega^s$ $(s = +, -)$ and define the broken Sobolev space

$$PW^{k,p}(\tilde{\Omega}) = \{u : u|_{\tilde{\Omega}^s} \in W^{k,p}(\tilde{\Omega}^s), s = +, -, u \text{ satisfies (1.1d)} - \text{(1.1g)}\}. \tag{2.1}$$

For $p = 2$, we denote $PW^{k,2}(\tilde{\Omega})$ by $PH^k(\tilde{\Omega})$. For matrix value functions $\mathbf{u}$ with $\mathbf{u}_{i,j} \in W^{k,p}(\tilde{\Omega})$, we denote the corresponding Sobolev space $\mathbf{W}^{k,p}(\tilde{\Omega})$ and define

$$\|\mathbf{u}\|_{\mathbf{W}^{k,p}(\tilde{\Omega})} = \sum_{i,j} \|\mathbf{u}_{ij}\|_{W^{k,p}(\tilde{\Omega})}. \tag{2.2}$$

Let $\mathcal{T}_h$ be a shape-regular [10] triangular mesh on Ω with mesh size $h = \max_{T \in \mathcal{T}_h}\{h_T\}$ where h_T is the diameter of the element $T \in \mathcal{T}_h$. Define the set of interface elements $\mathcal{T}_h^i = \{T \in \mathcal{T}_h : T \cap \Gamma \neq \emptyset\}$, and the non-interface elements $\mathcal{T}_h^n = \mathcal{T}_h \backslash \mathcal{T}_h^i$. For $T \in \mathcal{T}_h^i$, we let $T^{\pm} = T \cap \Omega^{\pm}$, and $\Gamma_T = \Gamma \cap T$.

Let $\mathcal{E}_h$ denote the set of all edges of the mesh $\mathcal{T}_h$, and $\mathring{\mathcal{E}}_h$ the interior edges. Denote $\mathcal{E}_h^i$ and $\mathcal{E}_h^n = \mathcal{E}_h \backslash \mathcal{E}_h^i$ the set of interface edges and non-interface edges, respectively. For each $e \in \mathcal{E}_h^i$, define $e^{\pm} = e \cap \Omega^{\pm}$. Let $\mathcal{F}_h^i$ be the set of edges belonging to interface elements. For any $e \in \mathring{\mathcal{E}}_h$ denote the adjacent elements by T_e^1 and T_e^2, and define their jump and average by

$$[\![w]\!]_e = w|_{T_e^1} - w|_{T_e^2}, \quad \{\!\{w\}\!\}_e = \frac{1}{2}\left(w|_{T_e^1} + w|_{T_e^2}\right). \tag{2.3}$$

The unit normal $\mathbf{n}_e$ is oriented from T_e^1 to T_e^2, and the tangent vector $\mathbf{t}_e$ is taken counterclockwise along e. These notations are illustrated in Figure 2.1.

We assume that the interface Γ is C^2 smooth and satisfies the following assumptions:

(H1) The interface Γ cannot intersect an edge of any element at more than two points unless the edge is part of Γ.

(H2) If Γ intersects the boundary of an element at two points, these intersection points must be on different edges of this element.

The smoothness of Γ ensures the following lemma holds:

Lemma 2.1 (r-tubular neighborhood)**.** *Let Γ be a regular, simple, $\mathcal{C}^2$ curve. For each point $X \in \Gamma$, let $N_x(r)$ to be the line segment of length $2r$ centered at x and perpendicular to Γ. Then, there exists $r > 0$ such that for any two points $X, Y \in \Gamma, X \neq Y$, the line segments $N_X(r)$ and $N_Y(r)$ are disjoint. We define the r-tubular neighborhood of Γ by $U_\Gamma(r) = \cup_{X\in\Gamma} N_X(r)$.*

As in most cases, our analysis in this paper is conducted on the mesh $\mathcal{T}_h$ with sufficiently small h. To make it precise, inspired by [31], we denote the radius of the tubular neighborhood of the interface Γ by r and then restrict $h < r/2$.

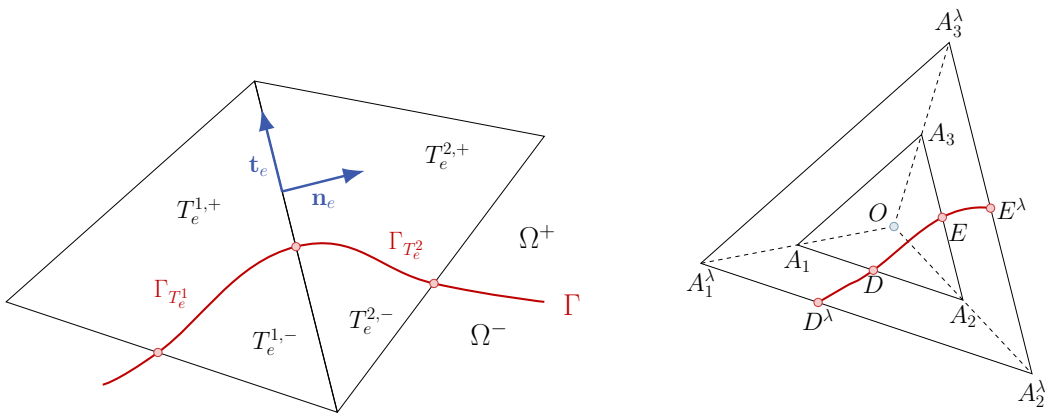

Figure 2.1: Notations of this article (Left) and fictitious element (Right)

3 High-Order Immersed FEM Space

In this section, we construct IFE spaces that approximately satisfy the biharmonic interface conditions (1.1d)-(1.1g).

3.1 Least-Squares Biharmonic IFE Spaces

For each triangular element $T \in \mathcal{T}_h$, let $\mathcal{P}_p(T)$ be the standard polynomial space of degree at most p on T. Let $\{A_i : i \in \mathcal{I}_p\}$ be the set of Lagrange nodes with set $\mathcal{N}_p(T) = \{A_i\}_{i\in\mathcal{I}_p}$ and $\mathcal{I}_p$ the index set. For example, when $p = 2$, we have $|\mathcal{I}_p| = 6$, with A_1, A_2, A_3 are vertices of T, and A_4, A_5, A_6 are midpoints of its edges.

On each non-interface element $T \in \mathcal{T}_h^n$, the local IFE space on T is identical to the standard Lagrange finite element space, i.e. $\mathcal{P}_p(T)$. Let $\psi_{i,T}^p \in \mathcal{P}_p(T)$ be the Lagrange shape functions such that

$$\psi_{i,T}^p(A_j) = \delta_{ij}, \quad \forall\ i, j \in \mathcal{I}_p,$$

where δ_{ij} is Kronecker delta function. In this case, the local IFE space on T is given by

$$S_h^p(T) := \text{span}\{\psi_{i,T}^p : i \in \mathcal{I}_p\}, \text{ for } T \in \mathcal{T}_h^n.$$

On each interface element $T \in \mathcal{T}_h^i$, the interface conditions are enforced in a least-squares sense. We denote $\mathcal{I}_p^{\pm} = \{i \in \mathcal{I}_p : A_i \in T^{\pm}\}$ the index set of Lagrange nodes located in $T^{\pm}$. Moreover, we define the tensor polynomial space $\mathcal{S}_p(T) = \mathcal{P}_p(T) \times \mathcal{P}_p(T)$ and the piecewise polynomial space

$$\mathcal{H}_p(T) = \{v \in L^2(T) : v|_{T^+} \in \mathcal{P}_p(T^+),\ v|_{T^-} \in \mathcal{P}_p(T^-)\}. \tag{3.1}$$

The spaces $\mathcal{S}_p(T)$ and $\mathcal{H}_p(T)$ are isomorphic, i.e., there exists a natural isomorphism $\mathcal{M}_T : \mathcal{S}_p(T) \to \mathcal{H}_p(T)$ given by

$$\mathcal{M}_T(u, v) = \begin{cases} u, \text{ on } T^+ \\ v, \text{ on } T^-, \end{cases} \quad \forall (u, v) \in \mathcal{S}_p(T). \tag{3.2}$$

The local IFE space on the interface element is constructed as a subspace of $\mathcal{H}_p(T)$. For ease of exposition, we construct the IFE space as a subspace of $\mathcal{S}_p(T)$ and then map into $\mathcal{H}_p(T)$ through $\mathcal{M}_T$. It is straightforward to verify that the following functions form a basis of $\mathcal{S}_p(T)$:

$$\xi_{i,T}^p = \begin{cases} \left(\psi_{i,T}^p, 0\right), \text{ if } i \in \mathcal{I}_p^+ \\ \left(0, \psi_{i,T}^p\right), \text{ if } i \in \mathcal{I}_p^-, \end{cases} \qquad \eta_{i,T}^p = \begin{cases} \left(0, \psi_{i,T}^p\right), \text{ if } i \in \mathcal{I}_p^+ \\ \left(\psi_{i,T}^p, 0\right), \text{ if } i \in \mathcal{I}_p^-. \end{cases} \tag{3.3}$$

We may write $\mathcal{S}_p = \mathcal{S}_{p,1} \oplus \mathcal{S}_{p,2}$ where $\mathcal{S}_{p,1} = \text{span}\{\xi_{i,T}^p, i \in \mathcal{I}_p\}$ and $\mathcal{S}_{p,2} = \text{span}\{\eta_{i,T}^p, i \in \mathcal{I}_p\}$. To enforce interface conditions, we define bilinear form $\mathcal{J}_\lambda^p(\cdot,\cdot) : \mathcal{S}_p(T) \times \mathcal{S}_p(T) \mapsto \mathbb{R}^+ \cup \{0\}$, which measures the violation of the interface conditions:

$$\begin{aligned} \mathcal{J}_\lambda^p(u, v) =& \omega_0 \int_{\Gamma_T^\lambda} [\![u]\!]\,[\![v]\!]\, ds + \omega_1 h^2 \int_{\Gamma_T^\lambda} [\![\partial_n u]\!]\,[\![\partial_n v]\!]\, ds + \omega_2 h^4 \int_{\Gamma_T^\lambda} [\![\beta\partial_{nn} u]\!]\,[\![\beta\partial_{nn} v]\!]\, ds \\ &+ \omega_3 h^6 \int_{\Gamma_T^\lambda} [\![\beta(\partial_n \Delta u + \partial_{ntt} u)]\!]\,[\![\beta(\partial_n \Delta v + \partial_{ntt} v)]\!]\, ds, \end{aligned} \tag{3.4}$$

here we adopted the idea of fictitious element introduced in [44], which constructs local IFE spaces on an enlarged element to alleviate ill-conditioning caused by extremely small-cut subelements. Specifically, for each $T \in \mathcal{T}_h^i$, we define the fictitious element

$$T_\lambda = \{X \in \mathbb{R}^2 : \exists Y \in T \text{ s.t. } \overrightarrow{OX} = \lambda \overrightarrow{OY}\},$$

where O is the barycenter of T. The extended interface segment is then $\Gamma_T^\lambda = T_\lambda \cap \Gamma$. An illustration of the fictitious element is show in the right hand side of Figure 2.1.

The bilinear functional $\mathcal{J}_\lambda^p(\cdot,\cdot)$ defines a semi-norm on $\mathcal{S}_p$, denoted by $|\cdot|_{\mathcal{J}_\lambda^p}$. In fact, for $p = 2$ or 3, it induces a norm, as will be shown later.

Given nodal values $\mathbf{v} = (v_i)_{i\in\mathcal{I}_p}$, the associated $\mathcal{S}_p$ IFE function on T takes the form

$$\varphi_T^p|_{\mathbf{v}} = \sum_{i\in\mathcal{I}_p} v_i \xi_{i,T}^p + \sum_{i\in\mathcal{I}_p} c_i \eta_{i,T}^p, \tag{3.5}$$

where the unknown coefficient vector $\mathbf{c} = (c_i)_{i\in\mathcal{I}_p}$ is determined by minimizing the violation of interface conditions $|\cdot|_{\mathcal{J}_\lambda^p}$. The precise statement is in Theorem 3.2. We test (3.5) against $\eta_{i,T}^p$ to enforce $\mathcal{J}_\lambda^p(\varphi_T^p|_{\mathbf{v}}, \eta_{i,T}^p) = 0$, $i = 1, 2, ..., |\mathcal{I}_p|$ leading to the following linear system:

$$\mathbf{A}^{p,\lambda}\mathbf{c} = -\mathbf{B}^{p,\lambda}\mathbf{v}, \tag{3.6}$$

with

$$\mathbf{A}_{ij}^{p,\lambda} = \left(\mathcal{J}_\lambda^p\left(\eta_{j,T}, \eta_{i,T}\right)\right)_{i,j\in\mathcal{I}_p} \in \mathbb{R}^{|\mathcal{I}_p|\times|\mathcal{I}_p|}, \quad \mathbf{B}_{ij}^{p,\lambda} = \left(\mathcal{J}_\lambda^p\left(\xi_{j,T}, \eta_{i,T}\right)\right)_{i,j\in\mathcal{I}_p} \in \mathbb{R}^{|\mathcal{I}_p|\times|\mathcal{I}_p|}. \tag{3.7}$$

The IFE functions of space $\mathcal{H}_p$ are then constructed by mapping $\varphi_T^p|_{\mathbf{v}}$ back via $\mathcal{M}_T$. In summary, the IFE basis functions on $T \in \mathcal{T}_h^i$ is defined by:

$$\phi_{i,T}^p := \mathcal{M}_T \varphi_T^p|_{\mathbf{e}_i}, \qquad i \in \mathcal{I}_p. \tag{3.8}$$

where $\mathbf{e}_i$ is the canonical basis vector in $\mathbb{R}^{|\mathcal{I}_p|}$. It is straightforward to verify $\phi_{i,T}^p(A_j) = \delta_{ij}$ for $i, j \in \mathcal{I}_p$. Examples of $\mathcal{P}_2$ and $\mathcal{P}_3$ IFE basis functions are shown in Figure 3.1. In the first row, the third, fifth and sixth $\mathcal{P}_2$ IFE basis functions are presented, while the second row lists the third, fifth and tenth $\mathcal{P}_3$ basis functions. It is clear that the pointwisely continuity of basis functions along the interface Γ_T cannot be guaranteed. In fact, enforcing two distinct polynomials to coincide pointwise on nontrivial curve is generally impossible. Instead, the IFE basis functions are weakly continuous across the interface.

For each $T \in \mathcal{T}_h$, we define the local finite element space $S_h^p(T)$ by:

$$S_h^p(T) := \begin{cases} \text{span}\{\psi_{i,T}^p,\ i \in \mathcal{I}_p\}, & \text{if } T \in \mathcal{T}_h^n \\ \text{span}\{\phi_{i,T}^p,\ i \in \mathcal{I}_p\}, & \text{if } T \in \mathcal{T}_h^i. \end{cases} \tag{3.9}$$

The global IFE space $S_h^p(\Omega)$ is then defined by

$$S_h^p(\Omega) = \left\{u \in L^2(\Omega) :\ u \text{ satisfies conditions } \textbf{(C1)-(C4)}\right\}. \tag{3.10}$$

where

- **(C1)** $u|_T \in S_h^p(T)$, for all $T \in \mathcal{T}_h$.
- **(C2)** u is continuous on every non-interface edge $e \in \mathcal{E}_h^n$.
- **(C3)** u is continuous at all nodals A_i, $i \in \mathcal{I}_p$ for all $T \in \mathcal{T}_h$.
- **(C4)** $u|_{\partial\Omega} = 0$.

Remark 3.1. *This least-squares functional (3.4) is sufficient for polynomial degree $p \le 3$. For higher degree such that $p \ge 4$, an appropriate extended jump conditions across interface needs to be employed in the least-squares functional.*

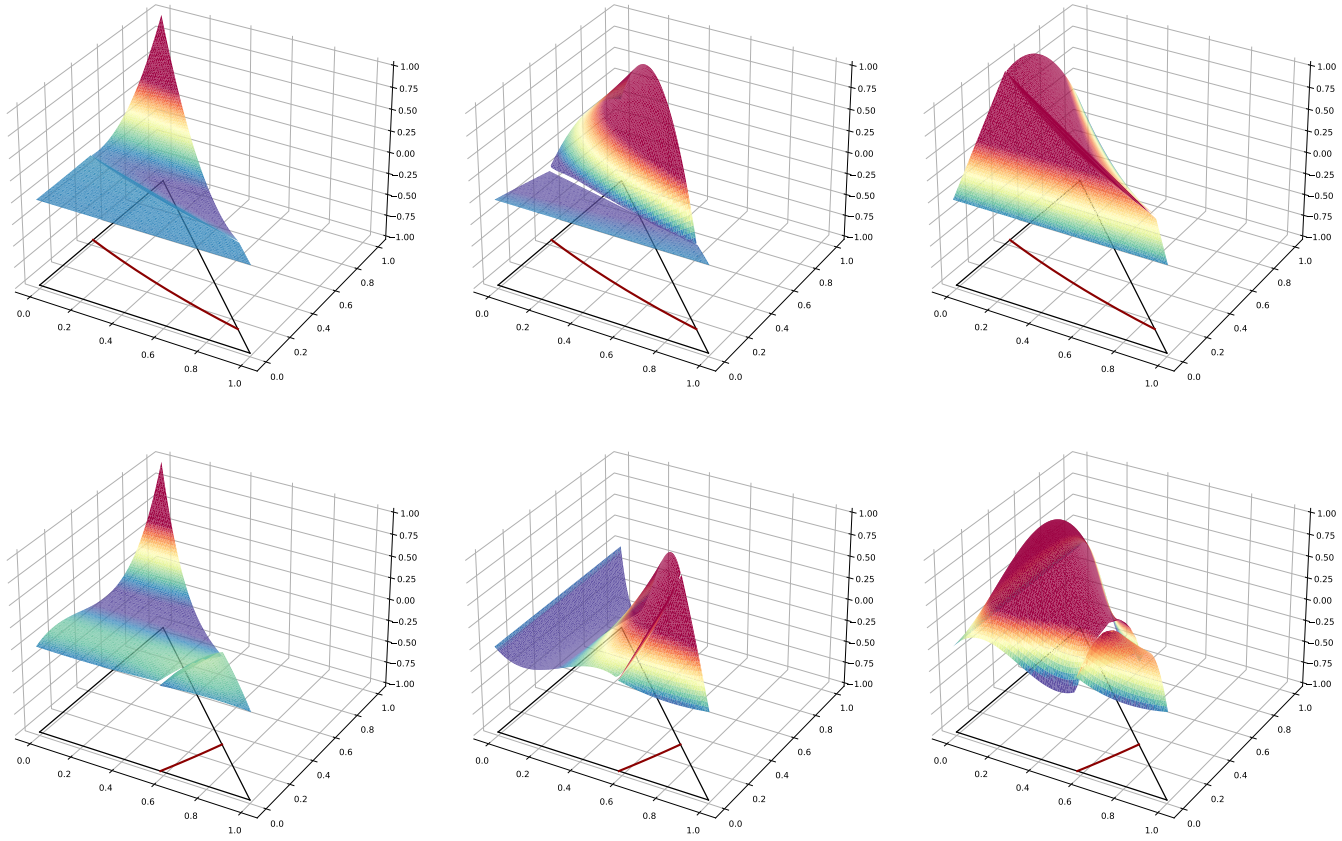

Figure 3.1: First Row: 3rd, 5th, 6th $\mathcal{P}_2$ basis functions; Second Row: 3rd, 5th, 10th $\mathcal{P}_3$ basis functions.

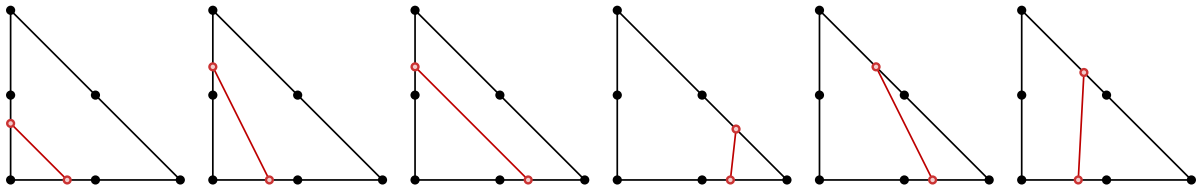

Figure 3.2: The exemplified cut cases when interface is a line. The sub-figures 1-3 are Type I elements for $\mathcal{P}_2$, the sub-figures 4-6 are Type II elements for $\mathcal{P}_2$.

3.2 Property of Biharmonic IFE Spaces

In this subsection, we present some basic properties for the biharmonic IFE space (3.9).

Theorem 3.1 (Unisolvence)**.** *On every interface element $T \in \mathcal{T}_h^i$, for polynomial degrees $p = 2$ and $p = 3$ with Γ not a straight line segment, given any nodal values $\mathbf{v}$, there exists a unique IFE shape function in the form of (3.5).*

Proof. The proof of existence follows arguments similar to Theorem 2.1 of [21]. For uniqueness, let $\mathcal{K}_\lambda^p$ denote the null space of $\mathcal{S}_{p,2}$. Then we prove the uniqueness in different categories of curve types for Γ_T^λ.

Case 1. Γ_T^λ *is a straight line.*

We consider $p = 2$ as an example. For this degenerate case, let $u = (u_1, u_2) \in \mathcal{S}_{p,2} \cap \mathcal{K}_\lambda^p$. Since $\mathbf{v} = \mathbf{0}$, we may write $u = \sum_{i=1}^{|\mathcal{I}|} c_i \eta_{i,T}$. Because Γ_T^λ is a line, the condition $u \in \mathcal{K}_\lambda^p$ implies

$$[\![u]\!] \equiv 0, \quad [\![\partial_n u]\!] \equiv 0, \quad [\![\beta \partial_{nn} u]\!] \equiv 0 \quad \text{and} \quad [\![\beta \left(\partial_n \Delta u + \partial_{ntt} u\right)]\!] \equiv 0$$

on Γ_T^λ. Equivalently, this yields a linear system $\mathbf{Mc} = \mathbf{0}$ where $\mathbf{M} \in \mathbb{R}^{|\mathcal{I}_p| \times |\mathcal{I}_p|}$. The structure of $\mathbf{M}$ depends on how the interface segment intersects the element T. If the interface passes through two legs of the right angle, T is called a type I element; otherwise, it is called a type II element. Some exemplified cutting configurations are illustrated in Figure 3.2. In each case, uniqueness follows by verifying that $\det(\mathbf{M}) \neq 0$ through direct computations. For instance, in the left configuration of Figure 3.2, the determinant can be explicitly written as:

$$det(\mathbf{M}) = 32(d^2 + e^2)^2(P_1 + \rho P_2) > 0 \tag{3.11}$$

where $1/2 \leq d \leq 1$ and $1/2 \leq e \leq 1$, $\rho = \beta^+/\beta^-$, and P_1 are P_2 are polynomial of d and e which cannot be equal to 0 at the same time:

$$\begin{aligned} P_1 =& -d^3(1-2e)^2 e - 2d^2(-2+e)e^3 - e^4 + de^3(-1+4e) + d^4(-1+4e-2e^2) \geq P_1(1/2, 1/2) \geq 1/8, \\ P_2 =& 2d^4(-1+e)^2 + d^3(1-2e)^2 e + 2d^2(-1+e)^2 e^2 + 2e^4 + d(e^3 - 4e^4) \geq P_2(1,1) \geq 0. \end{aligned} \tag{3.12}$$

The remaining case can be verified using the same logic, although the computation are tedious to included here. This proves the positive definiteness of $\mathcal{J}_\lambda^p$ on $\mathcal{S}_{p,2}$, which means $\mathcal{J}_\lambda^p(\cdot,\cdot)$ is an inner product on $\mathcal{S}_{p,2}$. Consequently, the matrix $\mathbf{A}$ is positive definite and therefore invertible.

Case 2. Γ_T^λ *is either a non-algebraic curve or an algebraic curve with degree greater than p.*

In this case, let $(u_1, u_2) \in \mathcal{S}_{p,2} \cap \mathcal{K}_\lambda^p$, then we claim that $(u_1, u_2) \equiv (0, 0)$. Indeed, note that $u_1 - u_2$ is a polynomial of degree at most p. It is impossible for such a polynomial to vanish almost everywhere on a non-algebraic curve, or an algebraic curve with degree greater than p. Therefore, we must have $u_1 - u_2 \equiv 0$ on T_λ, which implies $u_1 = u_2$. Since both vanish at all nodes A_i,$i \in \mathcal{I}_p$, it follows that $u_1 = u_2 \equiv 0$. Hence, $\mathcal{J}_\lambda^p(\cdot,\cdot)$ is an inner product on $\mathcal{S}_{p,2}$. Again, we conclude that $\mathbf{A}$ is positive definite and thus invertible.

Case 3. Γ_T^λ *is an algebraic curve of degree larger than $p/2$ but less than or equal to p.*

In this case, let $(u_1, u_2) \in \mathcal{S}_{p,2} \cap \mathcal{K}_\lambda$. We may write

$$u_1 - u_2 = L^k Q$$

where $L(x, y)$ is a polynomial whose zeros are given by Γ_T^λ and $k \geq 1$. Without loss of generality, assume that L is irreducible and relatively prime to the non-constant polynomial Q. Since $u_1 - u_2$ is of oder at most p and Γ_T^λ is of degree larger than $p/2$, we can only have $k < 2$, i.e. $k = 1$. Since $(u_1, u_2) \in \mathcal{K}_\lambda^p$, we must have

$$\partial_n (L^k Q) \equiv 0$$

on Γ_T^λ. By direct computation, we have

$$\partial_n L^k Q = k L^{k-1} \partial_n(L) Q + L^k \partial_n Q.$$

When $k = 1$, this reduces to $\partial_n LQ = (\partial_n L)Q$ on Γ_T^λ. Here, $(\partial_n Q)L = 0$ is due to $L = 0$ on Γ_T^λ. Since L and Q are relatively prime, it follows that $\partial_n L \equiv 0$ on Γ_T^λ. This implies $\partial_x L = \partial_y L = 0$ on Γ_T^λ, contradicting the assumption that Γ_T^λ is a nontrivial algebraic curve. Thus, the only possibility is $k = 0$ and $Q \equiv 0$, so that $u_1 - u_2 \equiv 0$ on T_λ. The remaining conclusion follows as in the previous cases. □

Remark 3.2. *For general polynomial order p, the construction based on the bilinear form (3.4) guarantees the existence of IFE shape functions. However, uniqueness can only be established when the interface curve is either non-algebraic or an algebraic curve of degree strictly greater than $p/2$. So for higher-order cases, it is natural to extend the interface jump conditions by incorporating additional terms in (3.4).*

Theorem 3.2 (Least Square Construction)**.** *On every interface element $T \in \mathcal{T}_h^i$, given nodal values $\mathbf{v}$, the IFE shape function constructed by the above procedure minimizes the semi norm $|\cdot|_{\mathcal{J}_\lambda^p}$ over $\mathcal{S}_p$.*

Proof. The proof follows the same argument as Theorem 2.2 in [21]. The property is a consequence of the least-squares construction of the IFE shape functions. □

Theorem 3.3 (Partition of Unity)**.** *On every interface element $T \in \mathcal{T}_h^i$, IFE basis functions satisfy the following partition of unity property:*

$$\sum_{i \in \mathcal{I}_p} \phi_{i,T}^p \equiv 1, \qquad p = 2, 3. \tag{3.13}$$

Proof. Let $\phi_T^p = \sum_{i \in \mathcal{I}_p} \phi_{i,T}^p$, so that $\mathcal{M}_T^{-1} \phi_T^p \in \mathcal{S}_p(T)$. By direct computation, we have

$$\phi_T^p(A_i) = 1, i \in \mathcal{I}_p$$

since $\phi_{i,T}^p(A_j) = \delta_{ij}$. This corresponds to the case $\mathbf{v} = \mathbf{1}$ in the IFE construction. By Theorem 3.1, there exists a coefficient vector $\mathbf{c}$ such that

$$\psi_T^p = \mathcal{M}_T^{-1} \phi_T^p, \quad \psi_T^p = \sum_{i \in \mathcal{I}_p} \xi_{i,T}^p + \sum_{i \in \mathcal{I}_p} c_i \eta_{i,T}^p. \tag{3.14}$$

It is clear that $\mathbf{c} = \mathbf{1}$ is a valid solution due to the partition of unity results of standard Lagrange type basis functions and the definitions of $\xi_{i,T}^p$ and $\eta_{i,T}^p$. By uniqueness result in Theorem 3.1, this solution is unique, so $\mathbf{c} = \mathbf{1}$. Therefore,

$$\phi_T^p = \mathcal{M}_T \left(\sum_{i \in \mathcal{I}_p} \xi_{i,T}^p + \sum_{i \in \mathcal{I}_p} \eta_{i,T}^p \right) \equiv 1, \text{ on } T. \tag{3.15}$$

□

4 Immersed C^0 Interior Penalty Method

In this section, we derive the immersed C^0 interior penalty scheme for the biharmonic interface problem.

4.1 Derivation of Immersed C^0 Interior Penalty Method

Let $u \in PH^4(\Omega)$ be the true solution of the problem (1.1). Define

$$V_h = \{v \in H_0^1(\Omega) : v|_T \in H^2(T) \ \text{ if } \ T \in \mathcal{T}_h^n, \ v|_{T^\pm} \in H^2(T^\pm) \ \text{ if } \ T \in \mathcal{T}_h^i\}. \tag{4.1}$$

On each interface element $T \in \mathcal{T}_h^i$, multiplying the equation (1.1a) by $v \in V_h$ and integrating by parts on the subelement T^s $(s = \pm)$ gives

$$\begin{aligned}\int_{T^s} \Delta\left(\beta\Delta u\right) v \ dX &= -\int_{T^s} \nabla v \cdot \left(\nabla\beta\Delta u\right) \ dX + \int_{\partial T^s} v\left(\nabla\beta\Delta u \cdot \mathbf{n}\right) \ ds \\ &= \int_{T^s} \beta\nabla^2 u : \nabla^2 v \ dX + \int_{\partial T^s} \beta\left(\partial_n\Delta u\right) v \ ds - \int_{\partial T^s} \beta\left(\nabla^2 u\right) : \left(\nabla v \otimes n\right) \ ds,\end{aligned} \tag{4.2}$$

where $(a \otimes b)_{ij} = a_i b_j$. After some simplification, we obtain

$$\int_{T^s} \left(\beta\Delta^2 u\right) v \ dX = \int_{T^s} \beta\nabla^2 u : \nabla^2 v \ dX + \int_{\partial T^s} \left[\beta\partial_n\Delta u v - \beta\partial_{nn} u\partial_n v - \beta\partial_{nt} u\partial_t v\right] ds. \tag{4.3}$$

Using the tangential derivative identity:

$$\int_{\partial T^s} \partial_{nt} u\partial_t v \ ds = \int_{\partial T^s} \partial_t\left(\partial_{nt} u v\right) \ ds - \int_{\partial T^s} \partial_{ntt} u v \ ds, \tag{4.4}$$

together with the gradient theorem

$$\int_{\partial T^s} \partial_t\left(\partial_{nt} u v\right) \ ds = 0. \tag{4.5}$$

The equation (4.3) becomes

$$\int_{T^s} \left(\beta\Delta^2 u\right) v \ dX = \int_{T^s} \beta\nabla^2 u : \nabla^2 v \ dX - \int_{\partial T^s} \beta\partial_{nn} u\partial_n v ds + \int_{\partial T^s} \beta\left(\partial_n\Delta u + \partial_{ntt} u\right) v ds. \tag{4.6}$$

Similarly, on non-interface elements $T \in \mathcal{T}_h^n$, it holds [11]

$$\int_T \left(\beta\Delta^2 u\right) v \ dX = \int_T \beta\nabla^2 u : \nabla^2 v \ dX - \int_{\partial T} \beta\partial_{nn} u\partial_n v ds + \int_{\partial T} \beta\left(\partial_n\Delta u + \partial_{ntt} u\right) v ds. \tag{4.7}$$

Summing (4.6) over $s = +, -$ and all interface elements $T \in \mathcal{T}_h^i$, together with summing (4.7) over all $T \in \mathcal{T}_h^n$, yields

$$\begin{aligned}\sum_{T\in\mathcal{T}_h} \int_T fv \ dX = &\sum_{T\in\mathcal{T}_h} \int_T \beta\nabla^2 u : \nabla^2 v \ dX \\ &- \sum_{e\in\mathring{\mathcal{E}}_h} \int_e \left\{\!\!\left\{\beta\partial_{nn} u\right\}\!\!\right\} \left[\!\left[\partial_n v\right]\!\right] ds + \sum_{e\in\mathring{\mathcal{E}}_h^i} \int_e \left\{\!\!\left\{\beta\left(\partial_n\Delta u + \partial_{ntt} u\right)\right\}\!\!\right\} \left[\!\left[v\right]\!\right] ds \\ &- \sum_{T\in\mathcal{T}_h^i} \int_{\Gamma_T} \left\{\!\!\left\{\beta\partial_{nn} u\right\}\!\!\right\} \left[\!\left[\partial_n v\right]\!\right] ds + \sum_{T\in\mathcal{T}_h^i} \int_{\Gamma_T} \left\{\!\!\left\{\beta\left(\partial_n\Delta u + \partial_{ntt} u\right)\right\}\!\!\right\} \left[\!\left[v\right]\!\right] ds.\end{aligned} \tag{4.8}$$

Finally, adding symmetric terms and stabilization terms following the convention of interior penalty methods, the immersed C^0 interior penalty Galerkin scheme for the biharmonic interface problem is defined as: find $u_h \in S_h^p(\Omega)$, such that:

$$a_h(u_h, v_h) = L_f(v_h), \quad \forall\ v_h \in S_h^p(\Omega), \tag{4.9}$$

where $a_h(u_h, v_h) = A_h(u_h, v_h) + J_{h,u}(u_h, v_h) + J_{h,n}(u_h, v_h)$. The components of $a_h(u_h, v_h)$ are given by

$$\begin{aligned}
A_h(u,v) &= \sum_{T\in\mathcal{T}_h} \int_T \beta \nabla^2 u : \nabla^2 v \, dX, \\
J_{h,u}(u,v) &= -\sum_{e\in\mathring{\mathcal{E}}_h} \int_e \{\!\{\beta \partial_{nn} u\}\!\} \, [\![\partial_n v]\!] \, ds - \sum_{e\in\mathring{\mathcal{E}}_h} \int_e \{\!\{\beta \partial_{nn} v\}\!\} \, [\![\partial_n u]\!] \, ds + \sum_{e\in\mathring{\mathcal{E}}_h^n} \frac{\sigma_u \beta}{|e|} \int_e [\![\partial_n u]\!] \, [\![\partial_n v]\!] \, ds \\
&\quad + \sum_{e\in\mathring{\mathcal{E}}_h^i} \left(\frac{\sigma_u \beta^+}{|e^+|} \int_{e^+} [\![\partial_n u]\!] \, [\![\partial_n v]\!] \, ds + \frac{\sigma_u \beta^-}{|e^-|} \int_{e^-} [\![\partial_n u]\!] \, [\![\partial_n v]\!] \, ds \right) + \sum_{T\in\mathcal{T}_h^i} \frac{\sigma_u \{\!\{\beta\}\!\}}{h_T} \int_{\Gamma_T} [\![\partial_n u]\!] \, [\![\partial_n v]\!] \, ds,
\end{aligned} \tag{4.10}$$

$$\begin{aligned}
J_{h,n}(u,v) &= \sum_{e\in\mathring{\mathcal{E}}_h^i} \sigma_F \left(|e^+|\beta^+ \int_{e^+} [\![\partial_{nn} u]\!] \, [\![\partial_{nn} v]\!] \, ds + |e^-|\beta^- \int_{e^-} [\![\partial_{nn} u]\!] \, [\![\partial_{nn} v]\!] \, ds \right) \\
&\quad + \sum_{e\in\mathring{\mathcal{E}}_h^n \cap \mathcal{F}_h^i} \sigma_F |e| \beta \int_e [\![\partial_{nn} u]\!] \, [\![\partial_{nn} v]\!] \, ds + \sum_{e\in\mathring{\mathcal{E}}_h^i} \frac{\sigma_n \{\!\{\beta\}\!\}}{|e|^3} \int_e [\![u]\!] \, [\![v]\!] \, ds + \sum_{T\in\mathcal{T}_h^i} \frac{\sigma_n \{\!\{\beta\}\!\}}{h_T^3} \int_{\Gamma_T} [\![u]\!] \, [\![v]\!] \, ds.
\end{aligned} \tag{4.11}$$

with $\{\!\{\beta\}\!\} = (\beta^+ + \beta^-)/2$. In this scheme, stabilization terms are included both on interface edges and interface segments, since the IFE space does not enforce the interface conditions pointwise. Inspired by [31], we further add penalty terms on the flux $\partial_n^2 u$ to enhance the numerical stability. These terms are applied to all edges of interface elements. A similar idea was employed in [21] where additional penalty terms were introduced to stabilize the pressure field in Stokes interface problems.

4.2 Well-posedness of the Numerical Solution

We establish the well-posedness of the numerical solution u_h obtained by the scheme (4.9). Define the mesh-dependent norm $\|\cdot\|_h$ on S_h^p by

$$\begin{aligned}
\|v\|_h^2 &= \sum_{T\in\mathcal{T}_h} \beta \|\nabla^2 v\|_{L^2(T)}^2 + \sum_{e\in\mathring{\mathcal{E}}_h^n} \frac{\sigma_u \beta}{|e|} \|[\![\partial_n v]\!]\|_{L^2(e)}^2 + \sum_{T\in\mathcal{T}_h^i} \frac{\sigma_u \{\!\{\beta\}\!\}}{h_T} \|[\![\partial_n v]\!]\|_{L^2(\Gamma_T)}^2 \\
&\quad + \sum_{e\in\mathring{\mathcal{E}}_h^i} \sigma_u \left(\frac{\beta^+}{|e^+|} \|[\![\partial_n v]\!]\|_{L^2(e^+)}^2 + \frac{\beta^-}{|e^-|} \|[\![\partial_n v]\!]\|_{L^2(e^-)}^2 \right) + \sum_{e\in\mathring{\mathcal{E}}_h^n \cap \mathcal{F}_h^i} \sigma_F |e| \beta \, \|[\![\partial_{nn} v]\!]\|_{L^2(e)}^2 \\
&\quad + \sum_{e\in\mathring{\mathcal{E}}_h^i} \sigma_F \left(|e^+|\beta^+ \, \|[\![\partial_{nn} v]\!]\|_{L^2(e^+)}^2 + |e^-|\beta^- \, \|[\![\partial_{nn} v]\!]\|_{L^2(e^-)}^2 \right) + \sum_{e\in\mathring{\mathcal{E}}_h^i} \frac{\sigma_n \{\!\{\beta\}\!\}}{|e|^3} \, \|[\![v]\!]\|_{L^2(e)}^2 \\
&\quad + \sum_{T\in\mathcal{T}_h^i} \frac{\sigma_n \{\!\{\beta\}\!\}}{h_T^3} \, \|[\![v]\!]\|_{L^2(\Gamma_T)}^2 .
\end{aligned} \tag{4.12}$$

Lemma 4.1. *$\|\cdot\|_h$ defines a norm on S_h^p.*

Proof. It is clear that $\|\cdot\|_h$ defines a semi-norm, so it remains to show positivity. Let $v \in S_h^p$ and assume $\|v\|_h = 0$. Then for each T for $\mathcal{T}_h^n$ and each each subelement $T^\pm$ with $\mathcal{T}_h^i$, we have $\|\nabla^2 v\|^2 = 0$. Hence, v is piecewise linear. By the definition of $\|\cdot\|_h$, the jump of v vanish across all non-interface edges, interface edges $e \in \mathcal{E}_h^i$, and interface segments Γ_T. Thus, v is continuous across the entire domain Ω. Similarly, the jumps of normal derivatives vanish, indicating v is globally linear. Since $v|_{\partial\Omega} = 0$ and Ω is a polygon domain, it follows that $v \equiv 0$. Hence $\|\cdot\|_h$ is a norm on S_h^p. □

Next we prove the trace inequality for IFE spaces. We first recall the standard trace inequality for a kth-degree polynomial v on a triangle T, with edge e [43]:

$$\|v\|_{L^2(e)} \leqslant \sqrt{\frac{(k+1)(k+2)}{2}\frac{|e|}{|T|}}\|v\|_{L^2(T)}. \tag{4.13}$$

Building on this estimate, we derive trace inequalities tailored to IFE functions on interface elements/edges.

Lemma 4.2. *Let $e \in \mathcal{E}_h^i$ be an interface edge with neighboring element T_e^1 and T_e^2. Suppose v is a polynomial of degree k. Then for $s = +, -$, there exists a constant C, independent of interface location and h, such that the following estimate holds for at least one of $i \in \{1, 2\}$:*

$$\|v\|_{L^2(e^s)} \leq C|e^s|^{-1/2}\|v\|_{L^2(T_e^{i,s})}. \tag{4.14}$$

Proof. Without loss of generality, consider the isosceles subtriangle $\tilde{T}_1 \subset T_e^{1,s}$ with base edge e^s and base angle $\tilde{\alpha} = \min\{\underline{\alpha}, \pi/4\}$, as constructed in the proof of Lemma 6 in [31] (see Figure 4.1). The existence of such a subtriangle is guaranteed by Lemma 2.1. Here, $\underline{\alpha}$ is the minimum nonzero angle of the triangulation whose existence is ensured by the shape regularity assumption on $\mathcal{T}_h$. Clearly, $\tilde{\alpha}$ is independent of the interface location. Applying the standard trace inequality on $\tilde{T}_1$, we obtain

$$\|v\|_{L^2(e^s)} \leqslant \sqrt{\frac{(k+1)(k+2)}{2}\frac{|e^s|}{|\tilde{T}_1|}}\|v\|_{L^2(\tilde{T}_1)} = \sqrt{\frac{2(k+1)(k+2)}{|e^s|\tan\tilde{\alpha}}}\|v\|_{L^2(T_e^{1,s})}. \tag{4.15}$$

The equality is due to $|\tilde{T}_1| = \frac{1}{4}|e^s|^2\tan(\tilde{\alpha})$. Setting $C = \sqrt{\frac{2(k+1)(k+2)}{\tan\tilde{\alpha}}}$, we obtain the estimate. The constant C depends only on the polynomial degree k and shape-regularity constant. □

Then we derive the following estimate for the symmetric term of (4.9) on interface edge.

Lemma 4.3. *Let $u, v \in S_h^p$. Then*

$$\begin{aligned}
&\Big|\sum_{e\in\mathring{\mathcal{E}}_h^i}\int_e \{\!\{\beta\partial_{nn}u\}\!\}\,[\![\partial_n v]\!]\,ds\Big| \\
\leq&\frac{1}{8}\Big(\sum_{T\in\mathcal{T}_h}\beta\|\nabla^2 u\|^2_{L^2(T)} + \sum_{e\in\mathring{\mathcal{E}}_h^i}\beta^+|e^+|\,\|[\![\partial_{nn}u]\!]\|^2_{L^2(e^+)} + \sum_{e\in\mathring{\mathcal{E}}_h^i}\beta^-|e^-|\,\|[\![\partial_{nn}u]\!]\|^2_{L^2(e^-)}\Big) \\
&+C\Big(\sum_{e\in\mathring{\mathcal{E}}_h^i}\frac{\beta^+}{|e^+|}\,\|[\![\partial_n v]\!]\|^2_{L^2(e^+)} + \sum_{e\in\mathring{\mathcal{E}}_h^i}\frac{\beta^-}{|e^-|}\,\|[\![\partial_n v]\!]\|^2_{L^2(e^-)}\Big),
\end{aligned} \tag{4.16}$$

where $C > 0$ is independent of the interface location and the mesh size h.

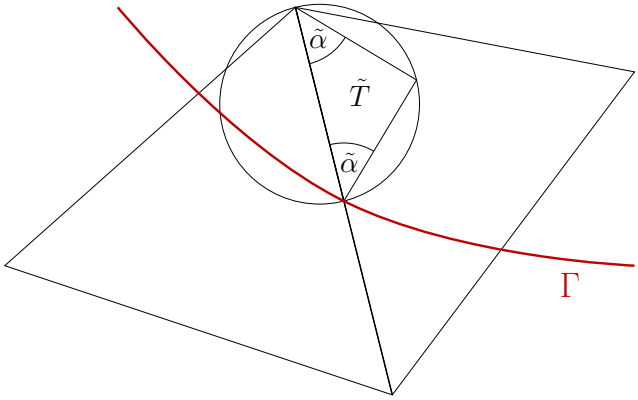

Figure 4.1: An illustration of triangular $\tilde{T}$

Proof. On the subedge e^+, we have the following equality:

$$\begin{aligned}\sum_{e\in\mathring{\mathcal{E}}_h^i}\int_{e^+}\{\!\{\beta\partial_{nn}u\}\!\}\,[\![\partial_n v]\!]\,ds &= \sum_{e\in\mathring{\mathcal{E}}_h^i}\int_{e^+}\left(\beta\partial_{nn}u\big|_{T_e^2}+\frac{1}{2}\,[\![\beta\partial_{nn}u]\!]\right)[\![\partial_n v]\!]\,ds\\ &= \sum_{e\in\mathring{\mathcal{E}}_h^i}\int_{e^+}\beta\partial_{nn}u\big|_{T_e^2}\,[\![\partial_n v]\!]\,ds+\frac{1}{2}\sum_{e\in\mathring{\mathcal{E}}_h^i}\int_{e^+}[\![\beta\partial_{nn}u]\!]\,[\![\partial_n v]\!]\,ds =: Q_1+Q_2.\end{aligned}\tag{4.17}$$

Without loss of generality, choose $T_e^{2,+}$ to be the subelement satisfying Lemma 4.2. Then by Cauchy-Schwarz inequality, we have

$$|Q_1|\le\left(\sum_{e\in\mathring{\mathcal{E}}_h^i}\beta^+|e^+|\left\|\partial_{nn}u\big|_{T_e^2}\right\|^2_{L^2(e^+)}\right)^{\frac{1}{2}}\left(\sum_{e\in\mathring{\mathcal{E}}_h^i}\frac{\beta^+}{|e^+|}\,\|[\![\partial_n v]\!]\|^2_{L^2(e^+)}\right)^{\frac{1}{2}}.\tag{4.18}$$

Applying Lemma 4.2 on $T_e^{2,+}$, we have

$$\begin{aligned}|Q_1|\le& C\left(\sum_{e\in\mathring{\mathcal{E}}_h^i}\beta^+\,\|\partial_{nn}u\|^2_{L^2(T_e^{2,+})}\right)^{\frac{1}{2}}\left(\sum_{e\in\mathring{\mathcal{E}}_h^i}\frac{\beta^+}{|e^+|}\,\|[\![\partial_n v]\!]\|^2_{L^2(e^+)}\right)^{\frac{1}{2}}\\ \le& C\left(\sum_{T\in\mathcal{T}_h^i}\beta^+\|\nabla^2 u\|^2_{L^2(T^+)}\right)^{\frac{1}{2}}\left(\sum_{e\in\mathring{\mathcal{E}}_h^i}\frac{\beta^+}{|e^+|}\,\|[\![\partial_n v]\!]\|^2_{L^2(e^+)}\right)^{\frac{1}{2}}.\end{aligned}\tag{4.19}$$

By Young's inequality $ab\le\frac{1}{8}a^2+2b^2$, we have

$$|Q_1|\le\frac{1}{8}\left(\sum_{T\in\mathcal{T}_h^i}\beta^+\|\nabla^2 u\|^2_{L^2(T^+)}\right)+2C^2\left(\sum_{e\in\mathring{\mathcal{E}}_h^i}\frac{\beta^+}{|e^+|}\,\|[\![\partial_n v]\!]\|^2_{L^2(e^+)}\right).\tag{4.20}$$

For Q_2, Cauchy-Schwarz and Young's inequality give

$$\begin{aligned}|Q_2| &\leq \frac{1}{2}\Big(\sum_{e\in\mathring{\mathcal{E}}_h^i}\beta^+|e^+|\,\|[\![\partial_{nn}u]\!]\|^2_{L^2(e^+)}\Big)^{\frac{1}{2}}\Big(\sum_{e\in\mathring{\mathcal{E}}_h^i}\frac{\beta^+}{|e^+|}\,\|[\![\partial_n v]\!]\|^2_{L^2(e^+)}\Big)^{\frac{1}{2}}\\ &\leq \frac{1}{8}\Big(\sum_{e\in\mathring{\mathcal{E}}_h^i}\beta^+|e^+|\,\|[\![\partial_{nn}u]\!]\|^2_{L^2(e^+)}\Big)+\frac{1}{2}\Big(\sum_{e\in\mathring{\mathcal{E}}_h^i}\frac{\beta^+}{|e^+|}\,\|[\![\partial_n v]\!]\|^2_{L^2(e^+)}\Big).\end{aligned} \tag{4.21}$$

Combine estimates of Q_1, Q_2, we have:

$$\begin{aligned}\Big|\sum_{e\in\mathring{\mathcal{E}}_h^i}\int_{e^+}\{\!\{\beta\partial_{nn}u\}\!\}\,[\![\partial_n v]\!]\,ds\Big| \leq &\frac{1}{8}\Big(\sum_{T\in\mathcal{T}_h^i}\beta^+\|\nabla^2 u\|^2_{L^2(T^+)}+\sum_{e\in\mathring{\mathcal{E}}_h^i}\beta^+|e^+|\,\|[\![\partial_{nn}u]\!]\|^2_{L^2(e^+)}\Big)\\ &+(2C^2+\frac{1}{2})\Big(\sum_{e\in\mathring{\mathcal{E}}_h^i}\frac{\beta^+}{|e^+|}\,\|[\![\partial_n v]\!]\|^2_{L^2(e^+)}\Big).\end{aligned} \tag{4.22}$$

An analogous estimate holds on e^-. Adding the two sides, we obtain the estimate (4.17). □

We have a similar estimate for the edges $e\in\mathring{\mathcal{E}}_h^n\cap\mathcal{F}_h^i$ neighbored by a non-interface element and interface element. This result is summarized in the following Lemma.

Lemma 4.4. *Let $u, v\in S_h^p$. Then*

$$\begin{aligned}\Big|\sum_{e\in\mathring{\mathcal{E}}_h^n\cap\mathcal{F}_h^i}\int_e\{\!\{\beta\partial_{nn}u\}\!\}\,[\![\partial_n v]\!]\,ds\Big| \leq &\frac{1}{8}\Big(\sum_{T\in\mathcal{T}_h}\beta\|\nabla^2 u\|^2_{L^2(T)}+\sum_{e\in\mathring{\mathcal{E}}_h^n\cap\mathcal{F}_h^i}\beta|e|\,\|[\![\partial_{nn}u]\!]\|^2_{L^2(e)}\Big)\\ &+C\sum_{e\in\mathring{\mathcal{E}}_h^n}\frac{\beta}{|e|}\,\|[\![\partial_n v]\!]\|^2_{L^2(e)}\,.\end{aligned} \tag{4.23}$$

where $C>0$ is independent of the interface location and the mesh size h.

Proof. For $e\in\mathring{\mathcal{E}}_h^n\cap\mathcal{F}_h^i$, at least one neighborhood element is a non-interface element. Without loss of generality, assume T_e^2 is non-interface. Then

$$\sum_{e\in\mathring{\mathcal{E}}_h^n\cap\mathcal{F}_h^i}\int_e\{\!\{\beta\partial_{nn}u\}\!\}\,[\![\partial_n v]\!]\,ds=\sum_{e\in\mathring{\mathcal{E}}_h^n\cap\mathcal{F}_h^i}\int_e\Big(\beta\partial_{nn}u\big|_{T_e^2}\Big)\,[\![\partial_n v]\!]\,ds+\frac{1}{2}\sum_{e\in\mathring{\mathcal{E}}_h^n\cap\mathcal{F}_h^i}\int_e[\![\beta\partial_{nn}u]\!]\,[\![\partial_n v]\!]\,ds=:Q_3+Q_4. \tag{4.24}$$

For Q_3, applying standard trace inequality similar to Lemma 4.2 and summing over all elements gives

$$|Q_3|\leq C\Big(\sum_{T\in\mathcal{T}_h}\beta\|\nabla^2 u\|^2_{L^2(T)}\Big)^{\frac{1}{2}}\Big(\sum_{e\in\mathring{\mathcal{E}}_h^n\cap\mathcal{F}_h^i}\frac{\beta}{|e|}\,\|[\![\partial_n v]\!]\|^2_{L^2(e)}\Big)^{\frac{1}{2}}. \tag{4.25}$$

For Q_4, Cauchy-Schwarz inequality gives

$$|Q_4|\leq\frac{1}{2}\Big(\sum_{e\in\mathring{\mathcal{E}}_h^n\cap\mathcal{F}_h^i}\beta|e|\,\|[\![\partial_{nn}u]\!]\|^2_{L^2(e)}\Big)^{\frac{1}{2}}\Big(\sum_{e\in\mathring{\mathcal{E}}_h^n\cap\mathcal{F}_h^i}\frac{\beta}{|e|}\,\|[\![\partial_n v]\!]\|^2_{L^2(e)}\Big)^{\frac{1}{2}}. \tag{4.26}$$

Applying Young's inequality to the bounds for Q_3 and Q_4 yields the estimate (4.23). □

Next we prove the continuity and coercivity for $a_h(u,v)$:

Theorem 4.1 (Continuity). *For all $u, v \in S_h^p$, there exists a constant C independent with the interface location such that:*

$$a_h(u,v) \leq C \|u\|_h \|v\|_h . \tag{4.27}$$

Proof. It suffices to bound the symmetric terms, since the other terms follow directly by Cauchy-Schwarz inequality. For $e \in \mathcal{E}_h^n \backslash \mathcal{F}_h^i$, the standard estimate [8] together with trace and inverse inequalities gives

$$\Big| \sum_{e\in\mathcal{E}_h^n\backslash\mathcal{F}_h^i} \int_e \{\!\{\beta\partial_{nn}u\}\!\} [\![\partial_n v]\!]\, ds \Big| \leq C \Big(\sum_{T\in\mathcal{T}_h} \beta \|\nabla^2 u\|^2_{L^2(T)} \Big)^{\frac{1}{2}} \Big(\sum_{e\in\mathring{\mathcal{E}}_h^n} \frac{\beta}{|e|} \|[\![\partial_n v]\!]\|^2 \Big)^{\frac{1}{2}} \leq C \|u\|_h \|v\|_h . \tag{4.28}$$

For $e \in \mathcal{E}_h^n \cap \mathcal{F}_h^i$, the bound follows from (4.25) and (4.26) . For $e \in \mathring{\mathcal{E}}_h^i$ we use (4.19) and (4.21). The stabilization terms in $J_{h,u}(u,v)$ and $J_{h,n}(u,v)$ are bounded by Cauchy-Schwarz inequality. Finally, for $A_h(u,v)$ we have

$$\Big| A_h(u,v) \Big| \leq \Big(\sum_{T\in\mathcal{T}_h} \beta \|\nabla^2 u\|^2_{L^2(T)} \Big)^{\frac{1}{2}} \Big(\sum_{T\in\mathcal{T}_h} \beta \|\nabla^2 v\|^2_{L^2(T)} \Big)^{\frac{1}{2}} \leq \|u\|_h \|v\|_h . \tag{4.29}$$

Combining all estimates gives the continuous result (4.27). □

Theorem 4.2 (Coercivity). *For all $v \in S_h^p$, there exists a constant c,, independent of the interface location, such that*

$$a_h(v,v) \geq c \|v\|_h^2 . \tag{4.30}$$

Proof. As before, we only need to estimate the symmetric terms. For $e \in \mathring{\mathcal{E}}_h^n \backslash \mathcal{F}_h^i$, the standard estimate yields

$$\begin{aligned} -\sum_{e\in\mathcal{E}_h^n\backslash\mathcal{F}_h^i} \int_e \{\!\{\beta\partial_{nn}v\}\!\} [\![\partial_n v]\!]\, ds &\geq -C \Big(\sum_{T\in\mathcal{T}_h} \beta \|\nabla^2 u\|^2_{L^2(T)} \Big)^{\frac{1}{2}} \Big(\sum_{e\in\mathring{\mathcal{E}}_h^n} \frac{\beta}{|e|} \|[\![\partial_n v]\!]\|^2 \Big)^{\frac{1}{2}} \\ &\geq -C \Big[\frac{1}{8C} \Big(\sum_{T\in\mathcal{T}_h} \beta \|\nabla^2 u\|^2_{L^2(T)} \Big) + 2C \Big(\sum_{e\in\mathring{\mathcal{E}}_h^n} \frac{2\{\!\{\beta\}\!\}_e}{|e|} \|[\![\partial_n v]\!]\|^2 \Big) \Big] \\ &\geq -\frac{1}{8} \Big(\sum_{T\in\mathcal{T}_h} \beta \|\nabla^2 u\|^2_{L^2(T)} \Big) - C \Big(\sum_{e\in\mathring{\mathcal{E}}_h^n} \frac{\{\!\{\beta\}\!\}_e}{|e|} \|[\![\partial_n v]\!]\|^2 \Big). \end{aligned} \tag{4.31}$$

For $e \in \mathcal{E}_h^n \cap \mathcal{F}_h^i$, Lemma 4.4 gives

$$\begin{aligned} &-\sum_{e\in\mathring{\mathcal{E}}_h^n\cap\mathcal{F}_h^i} \int_e \{\!\{\beta\partial_{nn}v\}\!\} [\![\partial_n v]\!]\, ds \\ &\geq -\frac{1}{8} \Big(\sum_{T\in\mathcal{T}_h} \beta \|\nabla^2 v\|^2_{L^2(T)} + \sum_{e\in\mathring{\mathcal{E}}_h^n\cap\mathcal{F}_h^i} \beta|e| \|[\![\partial_{nn} v]\!]\|^2_{L^2(e)} \Big) - C \Big(\sum_{e\in\mathring{\mathcal{E}}_h^n} \frac{\beta}{|e|} \|[\![\partial_n v]\!]\|^2_{L^2(e)} \Big). \end{aligned} \tag{4.32}$$

For $e \in \mathring{\mathcal{E}}_h^i$, we use Lemma 4.3 to get:

$$\begin{aligned}
&-\sum_{e\in\mathring{\mathcal{E}}_h^i}\int_e \{\!\{\beta\partial_{nn}v\}\!\}\,[\![\partial_n v]\!]\,ds \\
\geq&-\frac{1}{8}\Big(\sum_{T\in\mathcal{T}_h}\beta\|\nabla^2 v\|^2_{L^2(T)}+\sum_{e\in\mathring{\mathcal{E}}_h^i}\beta^+|e^+|\,\|[\![\partial_{nn}v]\!]\|^2_{L^2(e^+)}+\sum_{e\in\mathring{\mathcal{E}}_h^i}\beta^-|e^-|\,\|[\![\partial_{nn}v]\!]\|^2_{L^2(e^-)}\Big) \\
&-C\Big(\sum_{e\in\mathring{\mathcal{E}}_h^i}\frac{\beta^+}{|e^+|}\,\|[\![\partial_n v]\!]\|^2_{L^2(e^+)}+\sum_{e\in\mathring{\mathcal{E}}_h^i}\frac{\beta^-}{|e^-|}\,\|[\![\partial_n v]\!]\|^2_{L^2(e^-)}\Big).
\end{aligned} \tag{4.33}$$

Taking the generic C to be the maximum in the above three estimate, we have

$$\begin{aligned}
a_h(v,v)\geq&\frac{1}{4}\sum_{T\in\mathcal{T}_h}\beta\|\nabla^2 v\|^2_{L^2(T)}+(\sigma_u-2C)\sum_{e\in\mathring{\mathcal{E}}_h^n}\frac{\{\!\{\beta\}\!\}_e}{|e|}\,\|[\![\partial_n v]\!]\|^2+\sum_{T\in\mathcal{T}_h^i}\frac{\sigma_u\,\{\!\{\beta\}\!\}_e}{|h_T|}\,\|[\![\partial_n v]\!]\|^2_{L^2(\Gamma_T)} \\
&+(\sigma_u-C)\Big(\sum_{e\in\mathring{\mathcal{E}}_h^i}\frac{\beta^+}{|e^+|}\,\|[\![\partial_n v]\!]\|^2_{L^2(e^+)}+\sum_{e\in\mathring{\mathcal{E}}_h^i}\frac{\beta^-}{|e^-|}\,\|[\![\partial_n v]\!]\|^2_{L^2(e^-)}\Big) \\
&+(\sigma_F-\frac{1}{8})\Big(\sum_{e\in\mathring{\mathcal{E}}_h^n\cap\mathcal{F}_h^i}|e|\beta\,\|[\![\partial_{nn}v]\!]\|^2_{L^2(e)}+\sum_{e\in\mathring{\mathcal{E}}_h^i}\beta^+|e^+|\,\|[\![\partial_{nn}v]\!]\|^2_{L^2(e^+)}+\sum_{e\in\mathring{\mathcal{E}}_h^i}\beta^-|e^-|\,\|[\![\partial_{nn}v]\!]\|^2_{L^2(e^-)}\Big) \\
&+\sum_{e\in\mathring{\mathcal{E}}_h^i}\frac{\sigma_n\,\{\!\{\beta\}\!\}_e}{|e|^3}\,\|[\![v]\!]\|^2_{L^2(e)}+\sum_{T\in\mathcal{T}_h^i}\frac{\sigma_n\,\{\!\{\beta\}\!\}_e}{h_T^3}\,\|[\![v]\!]\|^2_{L^2(\Gamma_T)}\,.
\end{aligned} \tag{4.34}$$

Choosing $\sigma_u = 3C$, $\sigma_F = 1$, and defining With $c = \min\{\frac{1}{4}, 2C\}$, we have the coercivity result. □

The well-posedness of our numerical scheme follows directly from the continuity and coercivity results, and the Lax-Milgram Theorem.

5 Numerical Examples

In this section, we present three numerical examples to demonstrate the performance of the immersed C^0 interior penalty method. Throughout all computation, the computational domain is chosen as $\Omega = [-1,1]\times[-1,1]$.

The interface-unfitted triangular mesh $\mathcal{T}_h$ is constructed as follows: we first partition Ω into N^2 uniform squares with side length $h = 2/N$, and then subdivide each square into two triangles by its diagonals with the negative slope.

For the construction of the IFE shape functions, we set the parameters in the bilinear form (3.4) as $\omega_0 = \max\{\beta^+,\beta^-\}^2$ and $\omega_1 = \omega_2 = \omega_3 = 1$. Numerical quadratures on curve interface segments and curved subelements are carried out by suitable mappings onto line segment and standard triangles, respectively.

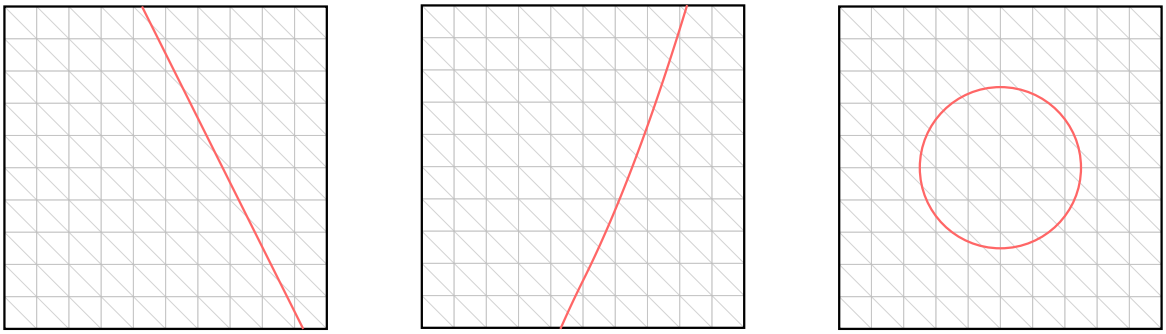

Figure 5.1: Illustration of interfaces used in Examples

5.1 Straight Line Interface

In this first example, we test the accuracy and consistency of proposed method with a straight line interface. The interface is represented by the level set

$$\Gamma = \{(x, y) \in \Omega : 2x + y - c = 0\},$$

which partitions the domain into $\Omega^+ = \{(x, y) \in \Omega : 2x + y - c > 0\}$ and $\Omega^- = \{(x, y) \in \Omega : 2x + y - c < 0\}$. The exact solution is given by

$$u(x, y) = \begin{cases} \frac{1}{\beta^-}(2x + y - c)^2 \sin^2(\pi y), & x \in \Omega^- \\ \frac{1}{\beta^+}(2x + y - c)^2 \sin^2(\pi y), & x \in \Omega^+. \end{cases} \tag{5.1}$$

In the following result, we take $c = \sqrt{0.5}$, see left plot of Figure 5.1 for a visualization.

Tables 1 and 3 report the interpolation errors of the $\mathcal{P}_2$ and $\mathcal{P}_3$ IFE spaces for the case $(\beta^-, \beta^+) = (1, 100)$. Both spaces exhibit optimal approximation order of convergence:

$$\|\mathcal{I}_h^p u - u\|_0 + h|\mathcal{I}_h^p u - u|_1 + h^2|\mathcal{I}_h^p u - u|_2 \approx \mathcal{O}(h^{p+1}), \quad p = 2, 3. \tag{5.2}$$

Tables 2 and Table 4 display the numerical solution errors. For $p = 2$, we observe optimal convergence in the H^1 and H^2-seminorms, and suboptimal convergence in L^2-norm, consistent with the known behavior of the C^0 interior penalty method for non-interface problems [26]. For $p = 3$, all norms convergence optimally, These results confirm that our immersed finite element spaces, combined with the proposed immersed C^0 interior penalty method, achieves the expected accuracy for the line interface case.

To further test the consistency with respect to the interface location, we consider a vertical interface aligned with y-axis. The new line interface can be written as

$$\Gamma = \{(x, y) : x - c = 0\}.$$

The exact solution is

$$u(x, y) = \begin{cases} \frac{1}{\beta^-}(x - c)^2 \sin^2(\pi y), & x \le c \\ \frac{1}{\beta^+}(x - c)^2 \sin^2(\pi y), & x > c \end{cases} \tag{5.3}$$

N	$\|\|\mathcal{I}_h^p u - u\|\|_0$	order	$\|\mathcal{I}_h^p u - u\|_1$	order	$\|\mathcal{I}_h^p u - u\|_2$	order
10	2.2981×10^{-2}		9.2168×10^{-1}		3.5313×10^{1}	
20	2.9230×10^{-3}	2.97	2.3391×10^{-1}	1.98	1.7926×10^{1}	0.98
40	3.6703×10^{-4}	2.99	5.8708×10^{-2}	1.99	8.9983×10^{0}	0.99
80	4.5932×10^{-5}	3.00	1.4692×10^{-2}	2.00	4.5036×10^{0}	1.00
160	5.7431×10^{-6}	3.00	3.6738×10^{-3}	2.00	2.2524×10^{0}	1.00

Table 1: Interpolation error of immersed $\mathcal{P}_2$ element of line interface when $\beta^+ = 100$, $\beta^- = 1$

N	$\|\|u_h - u\|\|_0$	order	$\|u_h - u\|_1$	order	$\|u_h - u\|_2$	order
10	1.1367×10^{-1}		1.0854×10^{0}		3.5853×10^{1}	
20	2.7870×10^{-2}	2.03	2.6715×10^{-1}	2.02	1.8030×10^{1}	0.99
40	7.2460×10^{-3}	1.94	6.7052×10^{-2}	1.99	9.0140×10^{0}	1.00
80	1.8531×10^{-3}	1.97	1.6832×10^{-2}	1.99	4.5059×10^{0}	1.00
160	4.6735×10^{-4}	1.99	4.2162×10^{-3}	2.00	2.2527×10^{0}	1.00

Table 2: Numerical solution errors of $\mathcal{P}_2$ element of line interface when $\beta^+ = 100$, $\beta^- = 1$

N	$\|\|\mathcal{I}_h^p u - u\|\|_0$	order	$\|\mathcal{I}_h^p u - u\|_1$	order	$\|\mathcal{I}_h^p u - u\|_2$	order
10	1.6860×10^{-3}		1.0195×10^{-1}		6.4074×10^{0}	
20	1.0708×10^{-4}	3.98	1.2934×10^{-2}	2.98	1.6289×10^{0}	1.98
40	6.7182×10^{-6}	3.99	1.6225×10^{-3}	2.99	4.0884×10^{-1}	1.99
60	1.3280×10^{-6}	4.00	4.8104×10^{-4}	3.00	1.8184×10^{-1}	2.00
80	4.2028×10^{-7}	4.00	2.0298×10^{-4}	3.00	1.0231×10^{-1}	2.00
100	1.7218×10^{-7}	4.00	1.0394×10^{-4}	3.00	6.5485×10^{-2}	2.00

Table 3: Interpolation error of immersed $\mathcal{P}_3$ element of line interface when $\beta^+ = 100$, $\beta^- = 1$

N	$\|\|u_h - u\|\|_0$	order	$\|u_h - u\|_1$	order	$\|u_h - u\|_2$	order
10	6.4599×10^{-3}		1.3698×10^{-1}		6.0325×10^{0}	
20	4.1086×10^{-4}	3.97	1.7319×10^{-2}	2.98	1.5031×10^{0}	2.00
40	2.7180×10^{-5}	3.92	2.1956×10^{-3}	2.98	3.7432×10^{-1}	2.01
60	5.4620×10^{-6}	3.96	6.5410×10^{-4}	2.99	1.6610×10^{-1}	2.00
80	1.7460×10^{-6}	3.96	2.7676×10^{-4}	2.99	9.3358×10^{-2}	2.00
100	7.1692×10^{-7}	3.99	1.4196×10^{-4}	2.99	5.9720×10^{-2}	2.00

Table 4: Numerical solution errors of $\mathcal{P}_3$ element of line interface when $\beta^+ = 100$, $\beta^- = 1$

In this experiment, we set $(\beta^-, \beta^+) = (1, 10)$ and fix the mesh size $h = 2/40 = 0.05$. The parameter c varies across the interval $[0.71, 0.79]$, so that the interface $\{x = c\}$ moves through grid columns. When $c = 0.75$, the interface align exactly with the mesh, and the immersed C^0 interior penalty method reduces to a standard C^0 interior penalty method. Figure 5.2 reports the error in three norms as the interface moves. The results demonstrates that the errors evolve smoothly with respect to the interface location, including at the degenerated case when the interface coincides with the mesh. This confirms the robustness and consistency of our method under interface movement.

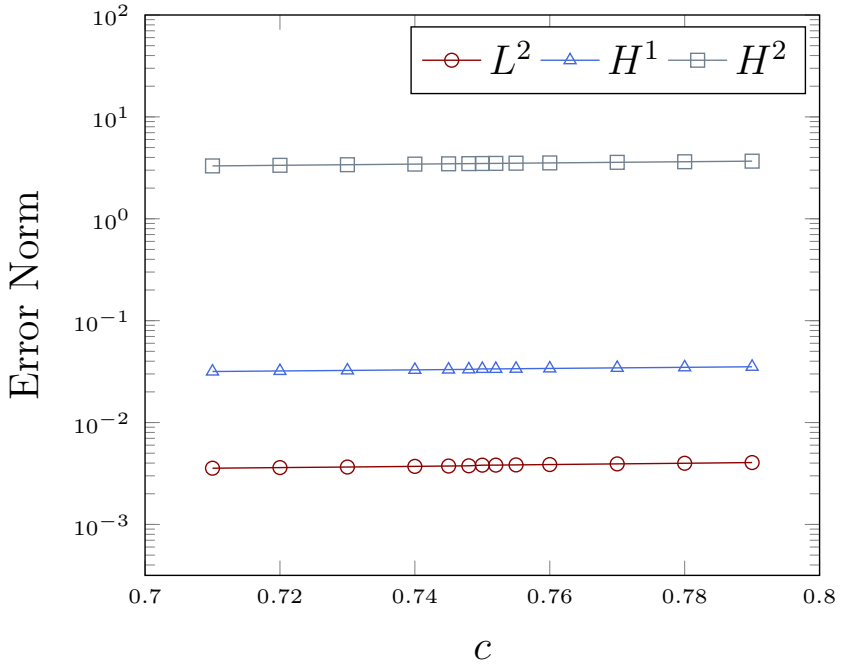

Figure 5.2: Errors of an moving line with respect to position

5.2 Parabola Interface Case

In this example, we test our method on a curved interface defined by a parabola. The interface is given by

$$\Gamma = \{(x, y) \in \Omega : y - (x^2 + 2x + c) = 0\}$$

which divides the domain into $\Omega^+ = \{(x, y) \in \Omega : y - (x^2 + 2x + c) > 0\}$ and $\Omega^- = \{(x, y) \in \Omega : y - (x^2 + 2x + c) < 0\}$. We set $c = -\frac{\sqrt{2}}{2}$ in the experiment, see the middle plot of Figure 5.1 for reference. The exact solution is defined by

$$u(x, y) = \begin{cases} \frac{1}{\beta^-}\left(x^2 + 2x + c - y\right)^2 \left(1 - y^2\right)^2, & x \in \Omega^-, \\ \frac{1}{\beta^-}\left(x^2 + 2x + c - y\right)^2 \left(1 - y^2\right)^2, & x \in \Omega^+. \end{cases} \tag{5.4}$$

Tables 5 and 6 report interpolation errors of the immersed $\mathcal{P}_2$ and $\mathcal{P}_3$ spaces for the case $\beta^+ = 10$ and $\beta^- = 1$. In both cases, we observe optimal convergence rates consistent with theoretical expectations.

N	$\|\|\mathcal{I}_h^p u - u\|\|_0$	order	$\|\mathcal{I}_h^p u - u\|_1$	order	$\|\mathcal{I}_h^p u - u\|_2$	order
10	5.8973×10^{-3}		2.5587×10^{-1}		8.2234×10^{0}	
20	7.5802×10^{-4}	2.96	6.6025×10^{-2}	1.95	4.2167×10^{0}	0.96
40	9.5420×10^{-5}	2.99	1.6647×10^{-2}	1.99	2.1224×10^{0}	0.99
80	1.1949×10^{-5}	3.00	4.1718×10^{-3}	2.00	1.0631×10^{0}	1.00
160	1.4944×10^{-6}	3.00	1.0437×10^{-3}	2.00	5.3187×10^{-1}	1.00

Table 5: Interpolation error of immersed $\mathcal{P}_2$ element of parabola interface when when $\beta^+ = 10$, $\beta^- = 1$

N	$\|\|\mathcal{I}_h^p u - u\|\|_0$	order	$\|\mathcal{I}_h^p u - u\|_1$	order	$\|\mathcal{I}_h^p u - u\|_2$	order
10	3.9532×10^{-4}		2.5529×10^{-2}		1.3731×10^{0}	
20	2.5089×10^{-5}	3.98	3.2559×10^{-3}	2.97	3.4956×10^{-1}	1.97
40	1.5807×10^{-6}	3.99	4.1044×10^{-4}	2.99	8.8171×10^{-2}	1.99
60	3.1153×10^{-7}	4.01	1.2152×10^{-4}	3.00	3.9124×10^{-2}	2.00
80	9.8835×10^{-8}	3.99	5.1370×10^{-5}	2.99	2.2057×10^{-2}	1.99
100	4.0438×10^{-8}	4.00	2.6281×10^{-5}	3.00	1.4101×10^{-2}	2.00

Table 6: Interpolation error of immersed $\mathcal{P}_3$ element of parabola interface when when $\beta^+ = 10$, $\beta^- = 1$

Figure 5.3 summarizes numerical solution errors for the parabola case with fixed $\beta^- = 1$ and varying β^+. When $\beta^+ = 1$, the interface disappears and the method reduces to the standard C^0 interior penalty method. In all cases, the proposed method achieves expected rates of convergence for both $\mathcal{P}_2$ and $\mathcal{P}_3$ spaces. The results also indicates mild variations in error magnitudes across different parameter values., but the convergence remains robust.

5.3 Circular Interface Case

In this example, we consider a circular interface. The interface is the level-set function

$$\Gamma = \{(x, y) \in \Omega : x^2 + y^2 = r_0^2\}.$$

which separates the domain into $\Omega^+ = \{(x, y) \in \Omega : x^2 + y^2 > r_0^2\}$ and $\Omega^- = \{(x, y) \in \Omega : x^2 + y^2 < r_0^2\}$. The exact solution is

$$u(x, y) = \begin{cases} \frac{\left(x^2+y^2-r_0^2\right)^2 \sin^2(\pi y)}{\beta^-}, & x \in \Omega^- \\ \frac{\left(x^2+y^2-r_0^2\right)^2 \sin^2(\pi y)}{\beta^+}, & x \in \Omega^+ \end{cases} \tag{5.5}$$

We take $r_0 = \pi/6.28$ in our tests, see the right plot of Figure 5.1 for reference.

Tables 7 and 9 report interpolation errors for $\beta^+ = 1$ and $\beta^- = 50$. As in previous examples, the immersed $\mathcal{P}_2$ and $\mathcal{P}_3$ spaces exhibit optimal approximation in $\|\cdot\|_0$, $|\cdot|_1$ and $|\cdot|_2$ norms. Tables 8 and 10 present the numerical solution errors for the proposed scheme.

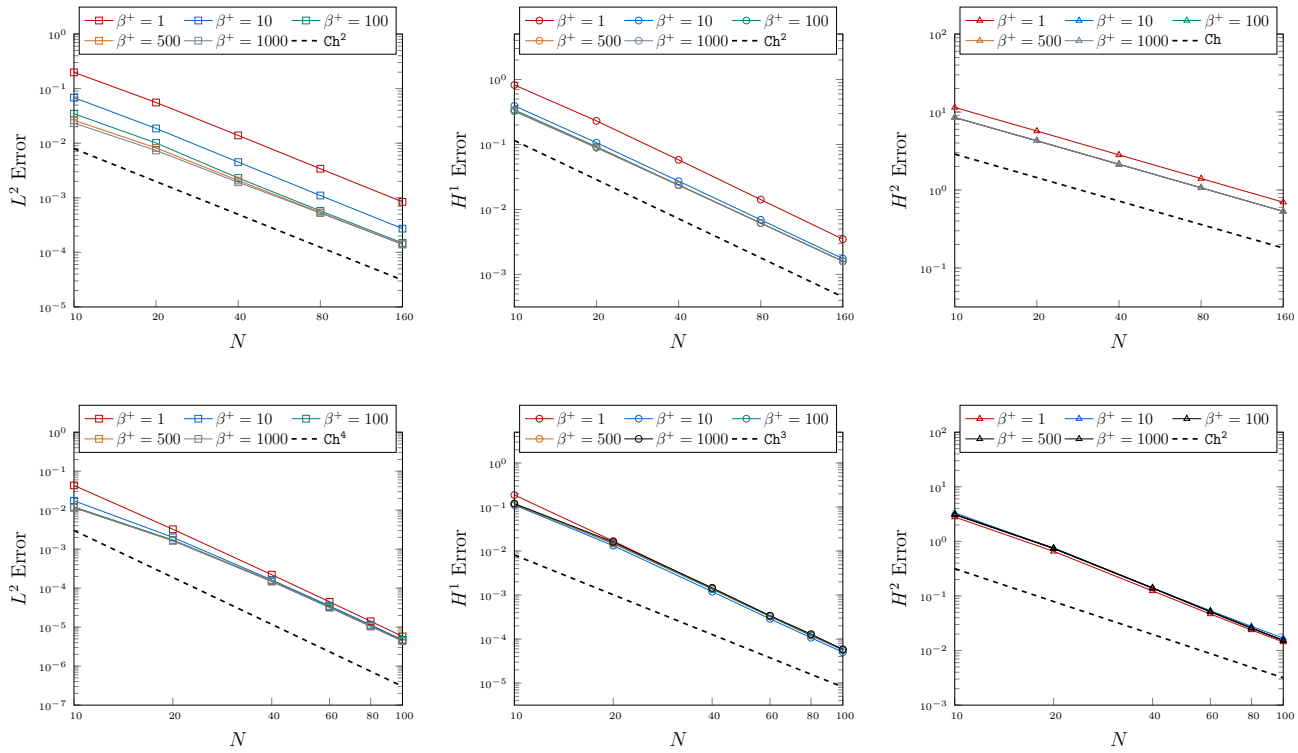

Figure 5.3: Numerical solution errors of $\mathcal{P}_2$ (first row) and $\mathcal{P}_3$ (second row) for parabola interface case

Finally, we examine the conditioning of the stiffness matrix associated with the scheme 4.9. Figure 5.4 shows condition number versus N for fixed $\beta^- = 1$ and varying β^+. For the $\mathcal{P}_2$ space (left), the condition number scales like $\mathcal{O}(h^{-4})$; moreover, the magnitude is higher for large coefficient jumps than for moderate ones. Similar behavior is observed for the immersed $\mathcal{P}_3$ space (right). These results indicate regular conditioning of the proposed method.

N	$\|\|\mathcal{I}_h^p u - u\|\|_0$	order	$\|\mathcal{I}_h^p u - u\|_1$	order	$\|\mathcal{I}_h^p u - u\|_2$	order
10	7.5156×10^{-3}		3.0133×10^{-1}		1.1212×10^{1}	
20	9.8140×10^{-4}	2.94	7.8906×10^{-2}	1.93	5.8092×10^{0}	0.95
40	1.2383×10^{-4}	2.99	1.9919×10^{-2}	1.99	2.9275×10^{0}	0.99
80	1.5514×10^{-5}	3.00	4.9916×10^{-3}	2.00	1.4666×10^{0}	1.00
160	1.9404×10^{-6}	3.00	1.2486×10^{-3}	2.00	7.3364×10^{-1}	1.00

Table 7: Interpolation error of immersed $\mathcal{P}_2$ element of circular interface when when $\beta^+ = 1$, $\beta^- = 50$

N	$\|\|u_h - u\|\|_0$	order	$\|u_h - u\|_1$	order	$\|u_h - u\|_2$	order
10	3.7308×10^{-2}		4.3174×10^{-1}		1.1364×10^{1}	
20	1.0019×10^{-2}	1.90	1.2319×10^{-1}	1.81	5.8557×10^{0}	0.96
40	2.9634×10^{-3}	1.76	3.4468×10^{-2}	1.84	2.9410×10^{0}	0.99
80	8.2261×10^{-4}	1.85	9.1887×10^{-3}	1.91	1.4702×10^{0}	1.00
160	2.1543×10^{-4}	1.93	2.3678×10^{-3}	1.96	7.3458×10^{-1}	1.00

Table 8: Numerical solution errors of $\mathcal{P}_2$ element of circular interface when $\beta^+ = 1$, $\beta^- = 50$

N	$\|\|\mathcal{I}_h^p u - u\|\|_0$	order	$\|\mathcal{I}_h^p u - u\|_1$	order	$\|\mathcal{I}_h^p u - u\|_2$	order
10	7.0400×10^{-4}		4.3002×10^{-2}		2.5482×10^{0}	
20	4.3799×10^{-5}	4.01	5.3550×10^{-3}	3.01	6.3730×10^{-1}	2.00
40	2.7397×10^{-6}	4.00	6.6977×10^{-4}	3.00	1.5955×10^{-1}	2.00
60	5.4131×10^{-7}	4.00	1.9849×10^{-4}	3.00	7.0938×10^{-2}	2.00
80	1.7129×10^{-7}	4.00	8.3747×10^{-5}	3.00	3.9910×10^{-2}	2.00
100	7.0169×10^{-8}	4.00	4.2880×10^{-5}	3.00	2.5545×10^{-2}	2.00

Table 9: Interpolation error of immersed $\mathcal{P}_3$ element of circular interface when when $\beta^+ = 1$, $\beta^- = 50$

5.4 A Flower Interface Case

In this final example, we consider a relatively complex flower-shaped interface. The level-set function of the interface is defined as

$$\phi(x, y) = (x^2 + y^2)[1 + 0.6 \sin(6 \arctan(y/x))] - (1.5\pi/6.28)^4,$$

which splits the domain into $\Omega^+ = \{(x, y) \in \Omega : \phi(x, y) > 0\}$ and $\Omega^- = \{(x, y) \in \Omega : \phi(x, y) < 0\}$. The shape of this interface is shown in the left plot of Figure 5.5. We set the source term $f = 0$ and homogenous boundary conditions.

Since it is difficult to construct an exact solution for this geometry, we adopt a reference solution $\hat{u}$ computed on a very fine mesh ($N = 320$) to evaluate errors. To facilitate high-order numerical quadrature on this irregular domain, we employ the technique described in [24, 41]. The computed errors for the

N	$\|\|u_h - u\|\|_0$	order	$\|u_h - u\|_1$	order	$\|u_h - u\|_2$	order
10	2.9512×10^{-2}		1.6345×10^{-1}		4.2294×10^{0}	
20	4.7377×10^{-3}	2.64	2.2606×10^{-2}	2.85	1.0358×10^{0}	2.03
40	2.0030×10^{-4}	4.56	2.0387×10^{-3}	3.47	2.1701×10^{-1}	2.25
60	4.3622×10^{-5}	3.76	5.0789×10^{-4}	3.43	8.4434×10^{-2}	2.33
80	1.4458×10^{-5}	3.84	1.8888×10^{-4}	3.44	4.3573×10^{-2}	2.30
100	6.0724×10^{-6}	3.89	8.8723×10^{-5}	3.39	2.6391×10^{-2}	2.25

Table 10: Numerical solution errors of $\mathcal{P}_3$ element of circular interface when $\beta^+ = 1$, $\beta^- = 50$

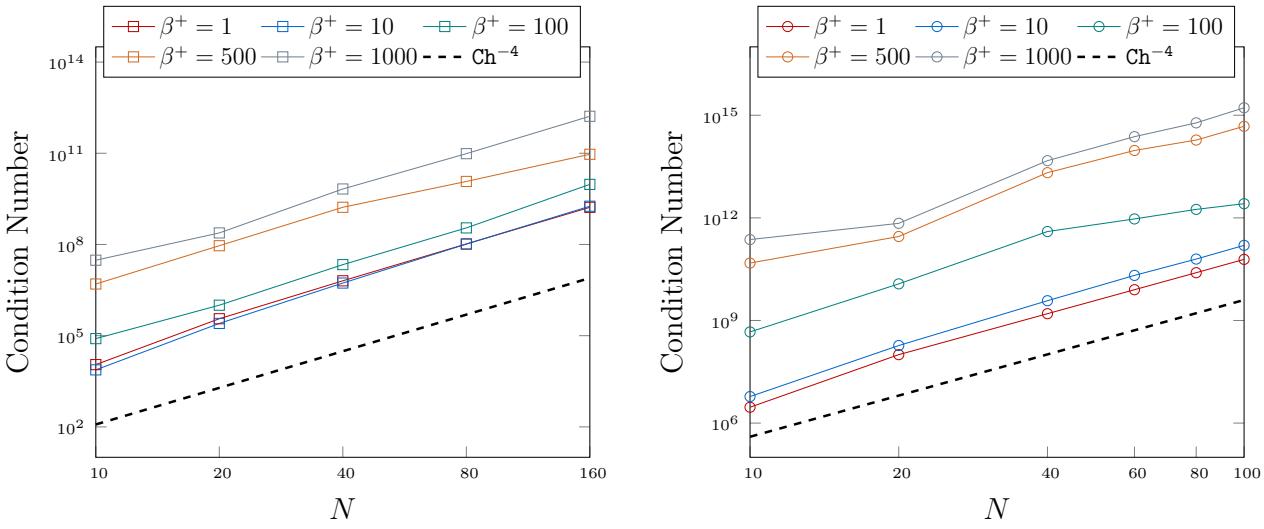

Figure 5.4: Condition number of $\mathcal{P}_2$ (left) and $\mathcal{P}_3$ (right) IPIFEM for circular interface case

immersed $\mathcal{P}_2$ C^0 interior penalty method are reported in Table 11. The approximate error norms are defined as

$$||u_h - \hat{u}||_{\tilde{0}} = h \left(\sum_{X \in \mathcal{N}_h} (u_h(X) - \hat{u}(X))^2 \right)^{1/2}, \quad |u_h - \hat{u}|_{\tilde{1}} = ||D_2 u_h - D_2 \hat{u}||_{\tilde{0}}, \tag{5.6}$$

where $D_2 u$ denotes the second-order central difference approximation of ∇u on the grid function u. The surface plot of the numerical solution is shown in the right plot of Figure 5.5.

N	$\|\|u_h - \hat{u}\|\|_{\tilde{0}}$	order	$\|u_h - \hat{u}\|_{\tilde{1}}$	order
10	2.9510×10^{-3}		4.8539×10^{-3}	
20	1.2720×10^{-3}	1.21	2.0239×10^{-3}	1.26
40	4.3351×10^{-4}	1.55	6.7660×10^{-4}	1.58
80	1.0786×10^{-4}	2.01	1.6779×10^{-4}	2.01
160	2.2620×10^{-5}	2.25	3.5572×10^{-5}	2.24

Table 11: Numerical solution errors of $\mathcal{P}_2$ element of flower interface when $\beta^+ = 1$, $\beta^- = 50$

6 Conclusion

In this paper, we developed immersed $\mathcal{P}_2$ and $\mathcal{P}_3$ finite element spaces for biharmonic interface problems. We analyzed key properties of these spaces, including unisolvence and the partition of unity. The number of degrees of freedom is identical to that of standard finite element spaces. The approximation capabilities

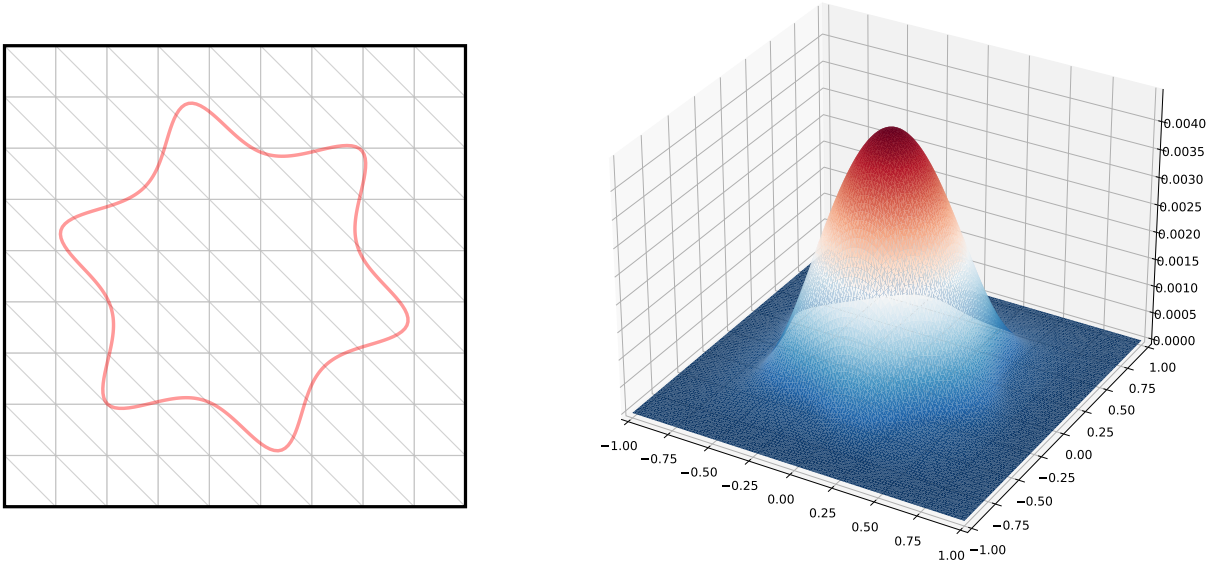

Figure 5.5: The shape (Left) and surface plot (Right) of the flower interface example

of the proposed spaces were confirmed to be optimal through numerical experiments. We further applied these spaces to solve biharmonic interface problem using an immersed C^0 interior penalty method, where additional penalty terms were introduced on both interior edges and interface segments to ensure stability and theoretical consistency. Extensive numerical experiments with various interface shapes demonstrated the optimal accuracy, robustness with respect to interface location, and regular conditioning of the proposed method.

References

[1] Slimane Adjerid, Ivo Babuška, Ruchi Guo, and Tao Lin. An enriched immersed finite element method for interface problems with nonhomogeneous jump conditions. *Comput. Methods Appl. Mech. Engrg.*, 404:Paper No. 115770, 37, 2023.

[2] Slimane Adjerid, Mohamed Ben-Romdhane, and Tao Lin. Higher degree immersed finite element spaces constructed according to the actual interface. *Comput. Math. Appl.*, 75(6):1868–1881, 2018.

[3] Slimane Adjerid, Ruchi Guo, and Tao Lin. High degree immersed finite element spaces by a least squares method. *Int. J. Numer. Anal. Model.*, 14(4-5):604–626, 2017.

[4] Slimane Adjerid, Tao Lin, and Haroun Meghaichi. A high order geometry conforming immersed finite element for elliptic interface problems. *Comput. Methods Appl. Mech. Engrg.*, 420:Paper No. 116703, 21, 2024.

[5] Slimane Adjerid, Tao Lin, and Haroun Meghaichi. The Frenet immersed finite element method for elliptic interface problems: an error analysis. *Comput. Methods Appl. Mech. Engrg.*, 438:Paper No. 117829, 19, 2025.

[6] John H Argyris, Isaac Fried, and Dieter W Scharpf. The tuba family of plate elements for the matrix displacement method. *The Aeronautical Journal*, 72(692):701–709, 1968.

[7] D. N. Arnold and F. Brezzi. Mixed and nonconforming finite element methods: implementation, postprocessing and error estimates. *RAIRO Modél. Math. Anal. Numér.*, 19(1):7–32, 1985.

[8] Susanne C Brenner. C0 interior penalty methods. In *Frontiers in Numerical Analysis-Durham 2010*, pages 79–147. Springer, 2011.

[9] Susanne C. Brenner and Ellya L. Kawecki. Adaptive C^0 interior penalty methods for Hamilton-Jacobi-Bellman equations with Cordes coefficients. *J. Comput. Appl. Math.*, 388:Paper No. 113241, 17, 2021.

[10] Susanne C. Brenner and L. Ridgway Scott. *The mathematical theory of finite element methods*, volume 15 of *Texts in Applied Mathematics*. Springer, New York, third edition, 2008.

[11] Susanne C. Brenner and Li-Yeng Sung. C^0 interior penalty methods for fourth order elliptic boundary value problems on polygonal domains. *J. Sci. Comput.*, 22/23:83–118, 2005.

[12] Susanne C. Brenner, Li-yeng Sung, and Yi Zhang. C^0 interior penalty methods for an elliptic state-constrained optimal control problem with Neumann boundary condition. *J. Comput. Appl. Math.*, 350:212–232, 2019.

[13] F. Brezzi. On the existence, uniqueness and approximation of saddle-point problems arising from Lagrangian multipliers. *Rev. Française Automat. Informat. Recherche Opérationnelle Sér. Rouge*, 8(R-2):129–151, 1974.

[14] Erik Burman, Peter Hansbo, and Mats G Larson. Cut bogner-fox-schmit elements for plates. *Advanced Modeling and Simulation in Engineering Sciences*, 7(1):27, 2020.

[15] Erik Burman, Peter Hansbo, and Mats G Larson. Cutfem based on extended finite element spaces. *Numerische Mathematik*, 152(2):331–369, 2022.

[16] Erik Burman, Peter Hansbo, Mats G Larson, and Sara Zahedi. Cut finite element methods. *Acta Numerica*, 34:1–121, 2025.

[17] Ying Cai, Jinru Chen, and Nan Wang. A Nitsche extended finite element method for the biharmonic interface problem. *Comput. Methods Appl. Mech. Engrg.*, 382:Paper No. 113880, 24, 2021.

[18] Ying Cai, Jinru Chen, and Nan Wang. A Nitsche mixed extended finite element method for the biharmonic interface problem. *Math. Comput. Simulation*, 203:112–130, 2023.

[19] Jiaqi Chen, Xufeng Xiao, and Xinlong Feng. A mixed immersed finite element method for fourth-order interface problems on surfaces. *Computers & Mathematics with Applications*, 176:122–139, 2024.

[20] Yan Chen, Ruo Li, and Qicheng Liu. An arbitrary order reconstructed discontinuous approximation to biharmonic interface problem. *arXiv preprint arXiv:2305.03430*, 2023.

[21] Yuan Chen and Xu Zhang. A P_2-P_1 partially penalized immersed finite element method for stokes interface problems. *Int. J. Numer. Anal. Model.*, 18(1):120–141, 2021.

[22] Yuan Chen and Xu Zhang. Solving Navier-Stokes equations with stationary and moving interfaces on unfitted meshes. *J. Sci. Comput.*, 98(1):Paper No. 19, 27, 2024.

[23] Yingda Cheng and Chi-Wang Shu. A discontinuous galerkin finite element method for time dependent partial differential equations with higher order derivatives. *Mathematics of computation*, 77(262):699–730, 2008.

[24] Tao Cui, Wei Leng, Huaqing Liu, Linbo Zhang, and Weiying Zheng. High-order numerical quadratures in a tetrahedron with an implicitly defined curved interface. *ACM Transactions on Mathematical Software (TOMS)*, 46(1):1–18, 2020.

[25] Amanda E Diegel and Natasha S Sharma. A c0 interior penalty method for the phase field crystal equation. *Numerical Methods for Partial Differential Equations*, 2020.

[26] G. Engel, K. Garikipati, T. J. R. Hughes, M. G. Larson, L. Mazzei, and R. L. Taylor. Continuous/discontinuous finite element approximations of fourth-order elliptic problems in structural and continuum mechanics with applications to thin beams and plates, and strain gradient elasticity. *Comput. Methods Appl. Mech. Engrg.*, 191(34):3669–3750, 2002.

[27] Richard S. Falk. Approximation of the biharmonic equation by a mixed finite element method. *SIAM J. Numer. Anal.*, 15(3):556–567, 1978.

[28] Ruchi Guo and Tao Lin. A higher degree immersed finite element method based on a Cauchy extension for elliptic interface problems. *SIAM J. Numer. Anal.*, 57(4):1545–1573, 2019.

[29] Ruchi Guo, Tao Lin, and Yanping Lin. Approximation capabilities of immersed finite element spaces for elasticity interface problems. *Numer. Methods Partial Differential Equations*, 35(3):1243–1268, 2019.

[30] Ruchi Guo and Xu Zhang. Solving three-dimensional interface problems with immersed finite elements: a-priori error analysis. *J. Comput. Phys.*, 441:Paper No. 110445, 23, 2021.

[31] Johnny Guzmán, Manuel A. Sánchez, and Marcus Sarkis. A finite element method for high-contrast interface problems with error estimates independent of contrast. *J. Sci. Comput.*, 73(1):330–365, 2017.

[32] Derrick Jones and Xu Zhang. A class of nonconforming immersed finite element methods for Stokes interface problems. *J. Comput. Appl. Math.*, 392:Paper No. 113493, 18, 2021.

[33] Zhilin Li and Fangfang Qin. An augmented method for 4th order PDEs with discontinuous coefficients. *J. Sci. Comput.*, 73(2-3):968–979, 2017.

[34] T. Lin, Y. Lin, W.-W. Sun, and Z. Wang. Immersed finite element methods for 4th order differential equations. *J. Comput. Appl. Math.*, 235(13):3953–3964, 2011.

[35] Tao Lin, Yanping Lin, and Xu Zhang. Partially penalized immersed finite element methods for elliptic interface problems. *SIAM J. Numer. Anal.*, 53(2):1121–1144, 2015.

[36] Tao Lin and Xu Zhang. Linear and bilinear immersed finite elements for planar elasticity interface problems. *J. Comput. Appl. Math.*, 236(18):4681–4699, 2012.

[37] Guodong Ma, Jinru Chen, and Feng Wang. A nitsche's extended nonconforming virtual element method for biharmonic pdes involving interfaces. *Computers & Mathematics with Applications*, 192:134–154, 2025.

[38] L. S. D. Morley. The triangular equilibrium element in the solution of plate bending problems. *Aero. Quart.*, 19(2):149–169, 1968.

[39] Igor Mozolevski, Endre Süli, and Paulo R. Bösing. *hp*-version a priori error analysis of interior penalty discontinuous Galerkin finite element approximations to the biharmonic equation. *J. Sci. Comput.*, 30(3):465–491, 2007.

[40] Lin Mu, Junping Wang, and Xiu Ye. Weak Galerkin finite element methods for the biharmonic equation on polytopal meshes. *Numer. Methods Partial Differential Equations*, 30(3):1003–1029, 2014.

[41] Robert I. Saye. High-order quadrature methods for implicitly defined surfaces and volumes in hyper-rectangles. *SIAM Journal on Scientific Computing*, 37(2):A993–A1019, 2015.

[42] Jin Wang, Xu Zhang, and Qiao Zhuang. An immersed Crouzeix-Raviart finite element method for Navier-Stokes equations with moving interfaces. *Int. J. Numer. Anal. Model.*, 19(4):563–586, 2022.

[43] T. Warburton and J. S. Hesthaven. On the constants in *hp*-finite element trace inverse inequalities. *Comput. Methods Appl. Mech. Engrg.*, 192(25):2765–2773, 2003.

[44] Qiao Zhuang and Ruchi Guo. High degree discontinuous Petrov-Galerkin immersed finite element methods using fictitious elements for elliptic interface problems. *J. Comput. Appl. Math.*, 362:560–573, 2019.